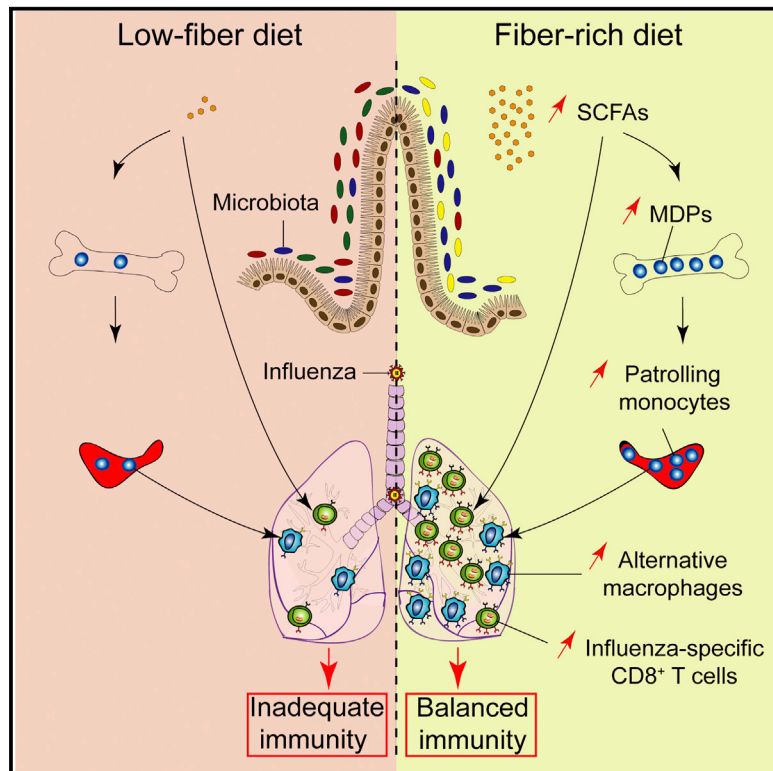


# Immunity

## Dietary Fiber Confers Protection against Flu by Shaping $\text{Ly6c}^-$ Patrolling Monocyte Hematopoiesis and $\text{CD8}^+$ T Cell Metabolism

### Graphical Abstract



### Authors

Aurélien Trompette, Eva S. Gollwitzer, Céline Pattaroni, ..., Lluís Fajas, Laurent P. Nicod, Benjamin J. Marsland

### Correspondence

benjamin.marsland@monash.edu

### In Brief

Trompette et al. report that a diet rich in the fermentable fiber inulin and the associated metabolites—short-chain fatty acids—improve the response of mice to influenza infection by dampening deleterious immunopathology caused by neutrophils while enhancing anti-viral  $\text{CD8}^+$  T cell responses through a boost in T cell metabolism.

### Highlights

- The fermentable fiber inulin and SCFAs protect against influenza-induced pathology
- SCFAs alter hematopoiesis by increasing macrophage precursors in the bone marrow
- SCFAs shape macrophage functionality to alleviate neutrophil-mediated tissue damage
- SCFAs enhance  $\text{CD8}^+$  T cell functionality by altering their metabolism



# Dietary Fiber Confers Protection against Flu by Shaping Ly6c<sup>-</sup> Patrolling Monocyte Hematopoiesis and CD8<sup>+</sup> T Cell Metabolism

Aurélien Trompette,<sup>1,5</sup> Eva S. Gollwitzer,<sup>1,3,5</sup> Céline Pattaroni,<sup>1,4</sup> Isabel C. Lopez-Mejia,<sup>2</sup> Erika Riva,<sup>1</sup> Julie Pernot,<sup>1</sup> Niki Ubags,<sup>1</sup> Lluís Fajas,<sup>2</sup> Laurent P. Nicod,<sup>1</sup> and Benjamin J. Marsland<sup>1,4,6,\*</sup>

<sup>1</sup>Faculty of Biology and Medicine, University of Lausanne, Service de Pneumologie, CHUV, CLED\_02.206, Chemin des Boveresses 155, 1066 Epalinges, Switzerland

<sup>2</sup>Department of Physiology, University of Lausanne, 1011 Lausanne, Switzerland; Center for Integrative Genomics (CIG), University of Lausanne, 1015 Lausanne, Switzerland

<sup>3</sup>Global Health Institute, EPFL-SV-GHI Station 19, EPFL, 1015 Lausanne, Switzerland

<sup>4</sup>Department of Immunology and Pathology, Monash University, Melbourne, Australia

<sup>5</sup>These authors contributed equally

<sup>6</sup>Lead Contact

\*Correspondence: [benjamin.marsland@monash.edu](mailto:benjamin.marsland@monash.edu)

<https://doi.org/10.1016/j.immuni.2018.04.022>

## SUMMARY

Dietary fiber protects against chronic inflammatory diseases by dampening immune responses through short-chain fatty acids (SCFAs). Here we examined the effect of dietary fiber in viral infection, where the anti-inflammatory properties of SCFAs in principle could prevent protective immunity. Instead, we found that fermentable dietary fiber increased survival of influenza-infected mice through two complementary mechanisms. High-fiber diet (HFD)-fed mice exhibited altered bone marrow hematopoiesis, characterized by enhanced generation of Ly6c<sup>-</sup> patrolling monocytes, which led to increased numbers of alternatively activated macrophages with a limited capacity to produce the chemokine CXCL1 in the airways. Blunted CXCL1 production reduced neutrophil recruitment to the airways, thus limiting tissue immunopathology during infection. In parallel, diet-derived SCFAs boosted CD8<sup>+</sup> T cell effector function by enhancing cellular metabolism. Hence, dietary fermentable fiber and SCFAs set an immune equilibrium, balancing innate and adaptive immunity so as to promote the resolution of influenza infection while preventing immune-associated pathology.

## INTRODUCTION

The beneficial effects of dietary fiber and its fermentation products, especially short-chain fatty acids (SCFAs), on a variety of chronic inflammatory diseases are well documented (Maslowski et al., 2009; Trompette et al., 2014). It has become evident that the impact of dietary fiber upon host immune responses goes beyond the gastrointestinal tract and can influence peripheral responses in tissues such as the lung and brain. Dietary fiber and SCFAs, notably acetate, propionate, and butyrate, can dampen

immune responses, acting on several different immune cells, including dendritic cells (DCs) (Millard et al., 2002; Trompette et al., 2014), macrophages (Chang et al., 2014; Millard et al., 2002), neutrophils (Vinolo et al., 2009), and regulatory T cells (Arpaia et al., 2013; Smith et al., 2013). SCFAs elicit their anti-inflammatory properties by either binding to G protein-coupled receptors (GPRs), principally FFAR3 (also known as GPR41) and FFAR2 (also known as GPR43) (Le Poul et al., 2003; Maslowski et al., 2009), or functioning as histone deacetylase (HDAC) inhibitors (Aoyama et al., 2010; Park et al., 2015). Moreover, SCFAs can influence cellular metabolism in liver, colonocytes, muscle, and adipose tissue (den Besten et al., 2013) via FFAR3 and FFAR2, by increasing AMP-activated protein kinase (AMPK) activity (Blad et al., 2012; den Besten et al., 2013; Hu et al., 2010) or by directly acting as a substrate for fatty acid oxidation (FAO) and gluconeogenesis (Blad et al., 2012; den Besten et al., 2013). Recent reports also point toward an involvement of SCFAs in immune cell metabolism (Kim et al., 2014); following conversion into acetyl-CoA and integration into the Krebs cycle (Blad et al., 2012; Donohoe et al., 2011; Kim et al., 2014), they can influence T helper cell differentiation via mTOR signaling (Kim et al., 2014) or accelerate recall responses of memory CD8<sup>+</sup> T cells (Balmer et al., 2016). Given the pleiotropic effects of SCFAs, it is key that conclusions are drawn from their function in specific physiologically relevant contexts—a particularly important point given the potential for development and use of SCFAs as therapeutics.

We have previously shown that mice consuming a diet high in fermentable fiber are protected against allergic airway inflammation. This protection is mediated by SCFAs, which, in a FFAR3-dependent manner, increase the accumulation of DCs in the airways that poorly present allergens to T cells. The consequence of this alteration in antigen presentation is a reduced Th2 cell response and better lung function (Trompette et al., 2014). However, whether this impaired induction of Th2 cell responses is reflective of a general dampening of inflammation, and thus potentially an increased susceptibility to infections, is unknown. Influenza A infection is one of the most common viral diseases worldwide, annually infecting 5%–20% of the population and responsible for substantial morbidity and mortality



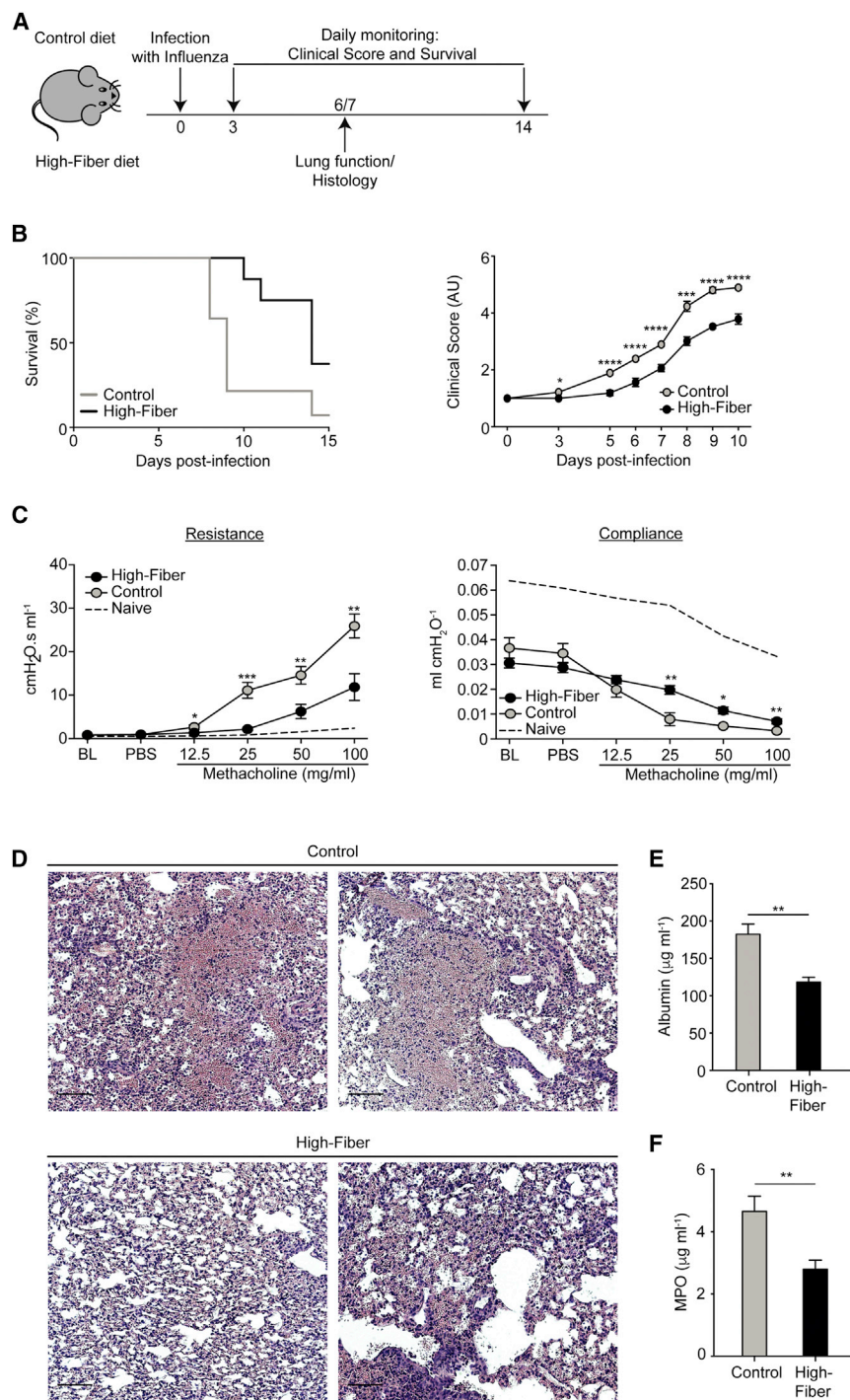


### Figure 1. Dietary Fiber Protects against Influenza-Induced Immunopathology

(A) Experimental model of high-dose influenza infection in control and high-fiber diet (HFD)-fed mice.

(B) Survival ( $p = 0.0101$ ) and clinical score of mice fed a control or HFD during the course of high-dose infection. AU, arbitrary units.

(C) Pulmonary resistance and compliance in response to methacholine in control and HFD-fed mice 7 days after high-dose infection.

(D) Representative hematoxylin and eosin (H&E)-stained lung tissue from mice on either control or HFD on day 7 after high-dose infection. Scale bars, 100  $\mu\text{m}$ .

(E) Quantification of albumin in the broncho-alveolar lavage fluid (BALF) of mice fed a control or HFD 7 days after high-dose infection.

(F) Myeloperoxidase (MPO) levels in the BALF of mice fed a control or HFD 7 days after high-dose infection.

Results are pooled from two independent experiments in (B) and representative of data generated in two independent experiments in (C)–(F). All results are expressed as mean  $\pm$  SEM;  $n = 8$ –14 per group in (B);  $n = 5$ –9 per group in (C)–(F). Statistical significance was determined with Mantel-Cox test for the survival in (B) and with Student's  $t$  test (unpaired, two-tailed) in (B)–(F). \* $p = 0.05$ , \*\* $p = 0.01$ , \*\*\* $p = 0.001$ , \*\*\*\* $p = 0.0001$ .

(WorldHealthOrganization, 2016). Here, we found that dietary fiber and SCFAs convey protection against influenza virus infection through two distinct pathways. A high-fiber diet resulted in altered bone marrow hematopoiesis, leading to the accumulation of alternatively activated macrophages (AAMs) in the lung of influenza-infected mice. These macrophages produced less CXCL1, effectively reducing early neutrophil infiltration into the airways and, hence, avoiding exaggerated tissue damage. Fermentation of dietary fiber also boosted CD8<sup>+</sup> T cell meta-

bolism and viral clearance. FFAR3 was required for the protective effect, and oral administration of SCFAs was sufficient to confer protection. The positive effects of dietary fiber in the development of protective immunity and reduced immune-mediated pathology upon influenza infection argue for further research in the use of SCFAs for the prevention and treatment of viral infections.

## RESULTS

### Dietary Fiber Protects against Influenza-Induced Pathology

A diet rich in fiber is known to improve intestinal health and to reduce inflammation both in the gut and in peripheral tissues such as the lung (Maslowski et al., 2009; Trompette et al., 2014); however, the consequences of this immuno-

modulation on protective immunity are unknown. To address whether fermentable dietary fiber influences antiviral immunity, mice were born and raised on a low-fiber diet (<0.3% crude fiber) supplemented with either cellulose (control) or inulin (high fiber; HFD). Cellulose is a poorly fermentable fiber and was used as a control to account for potential alterations in mineral and vitamin uptake. We then exposed adult mice to influenza A virus via the intranasal route and monitored them over the course of the infection (Figure 1A). Mice fed a HFD showed prolonged

survival and an ameliorated clinical score (Figure 1B). Moreover, HFD-fed mice exhibited reduced pulmonary resistance and increased compliance in response to methacholine (Figure 1C), corresponding to milder constriction of the airways, enhanced elasticity and, thus, better lung function. Histological analysis of the lung revealed extensive accumulation of red blood cells within the tissue of control mice (Figure 1D), indicating tissue destruction and vascular leakage. Higher albumin levels in the broncho-alveolar lavage fluid (BALF) of control mice (Figure 1E) supported this conclusion. However, this phenomenon and the associated worsened morbidity and mortality could not be attributed to epithelial cell destruction due to increased viral load in control animals (data not shown). Myeloperoxidase (MPO) activity, a well-known contributor to immunopathology in this model, was decreased in HFD-fed mice (Figure 1F). Thus, HFD-fed mice were protected against influenza-induced tissue destruction and lethality.

### The Dietary Fiber Inulin Alters the Intestinal Microbiota and Exhibits Butyrogenic Properties

Dietary fiber content can shape the composition of the gut microbiota (Carmody et al., 2015; De Filippo et al., 2010; Holscher et al., 2015; Martínez et al., 2010; Trompette et al., 2014). We thus characterized the intestinal microbiota of mice fed the inulin-rich HFD and compared this to the microbiota of mice fed the control cellulose-rich diet. To achieve this, we collected fecal pellets from mice given the respective diets and sequenced 16S ribosomal RNA gene (rRNA) amplicons. We found that inulin supplementation led to a marked alteration of the gut microbiota. Global community composition at the phylum level indicated that Bacteroidetes predominantly colonized mice fed either diet. However, while the control diet-fed mice had a microbiota dominated by the Rikenellaceae family, the HFD induced a considerable increase in the proportion of Bacteroidaceae together with a reduction in the numbers of operational taxonomic units (OTUs) belonging to the Firmicutes phylum (Figure 2A). We next aimed to identify bacterial OTUs whose relative abundance significantly differed among groups, even at low overall relative abundance. This approach revealed that feeding mice with the inulin-rich HFD stimulated the growth of certain communities, notably from the Bifidobacterium and Bacteroides genus (Figure 2B). Principal coordinates analysis (PCoA) on Bray Curtis distance showed significant separation of groups with approximately 56% variability explained by dietary fiber content (ANOSIM  $R^2 = 0.27$ ,  $p$  value = 0.00794), indicating that dietary fiber consumption led to significantly distinct microbial communities (Figure 2C). However, HFD did not alter the intestinal microbiota richness or diversity when compared to the control diet (Figure 2D). Bacterial fermentation of dietary fiber is known to result in the production of SCFAs, principally acetate, propionate, and butyrate (Cummings, 1981). Hence, we quantified SCFA levels present in the feces of mice fed the control diet or the HFD. We found that HFD altered the relative proportions of SCFAs, most notably that of butyrate (1.3% of the total SCFAs in control as compared to 11.2% in the HFD-fed mice) (Figure 2E). Absolute quantification revealed that HFD stimulated the local production of all three SCFAs, with a strong augmentation for butyrate (acetate, 1.82-fold over control; propionate,

1.39-fold over control; butyrate, 138.5-fold over control) (Figure 2E). We also found a significant increase of circulating, systemically available, SCFAs when mice were fed the HFD, with butyrate once more displaying the most robust increase comparable to what was seen in the intestine (Figure 2F). We next investigated whether SCFAs were sufficient to protect mice against infection. Given the significant increase in butyrate, we chose to concentrate on this specific SCFA, but similar data could be obtained when giving mice propionate (data not shown). We found that supplementing the drinking water with butyrate for 2 weeks prior to and throughout the infection resulted in protection similar to that elicited by a HFD (Figure 2G). Histological analysis of the lung revealed that mice treated with butyrate had significantly fewer inflammatory infiltrates in the airways, reduced tissue and vascular disruption, and subsequently less hemorrhaging (Figure 2H).

### Dietary Fiber Intake Prevents Excessive Neutrophil Influx into the Airways by Blunting the Levels of CXCL1 Produced by Lung Monocytes and Macrophages

To elucidate the immunological mechanisms underlying the protective effect of HFD, we assessed the immune response following a sublethal influenza infection in HFD-fed and control animals. During the early phase of infection, viral titers were equal or trending higher in HFD-fed mice (Figure 3A), an observation we also noted in the high-dose infection model (data not shown). Neutrophils have been linked to immunopathology and tissue damage (Kruger et al., 2015) and represent a high proportion of the immune cells infiltrating the lung early during viral infection (Perrone et al., 2008). We thus assessed the neutrophil influx into the airways. HFD-fed animals had lower numbers of neutrophils in the BALF throughout infection, and particularly at day 5 (Figure 3B), which marks the peak of neutrophilia in both groups, ruling out a delayed neutrophilic response in HFD-fed animals. This decreased neutrophil influx could be reproduced with SCFAs, as butyrate supplementation in drinking water also prevented excessive neutrophilia 5 days after infection (Figure 3C). Dietary fiber and SCFAs can exert their functions via multiple pathways, including binding to FFAR3 and FFAR2 (Le Poul et al., 2003; Maslowski et al., 2009). To elucidate whether the effect of dietary fiber on neutrophil recruitment upon influenza infection was dependent on one of these receptors, wild-type, *Ffar3*<sup>-/-</sup>, and *Ffar2*<sup>-/-</sup> mice were bred and raised on a control or HFD. Wild-type and *Ffar2*<sup>-/-</sup> mice showed reduced neutrophil infiltration into the airways 5 days after infection (Figure 3D). In contrast, there was no difference in neutrophil recruitment between *Ffar3*<sup>-/-</sup> mice fed a control or HFD (Figure 3D), indicating an involvement of FFAR3 in the blunted neutrophil response. We next determined whether this attenuated neutrophilic response was responsible for the increased survival observed in mice fed a HFD, a phenomenon that has been recently described by Brandes et al. (2013). To achieve this, we diminished pulmonary neutrophilia during the early phase of influenza infection by 50% using an anti-Ly6G antibody (Figure 3E), a reduction similar to what was observed in the HFD-fed or butyrate-treated animals (Figure 3B and 3C). Control mice on water that had reduced neutrophil numbers showed a significantly prolonged survival and better clinical score than mice that

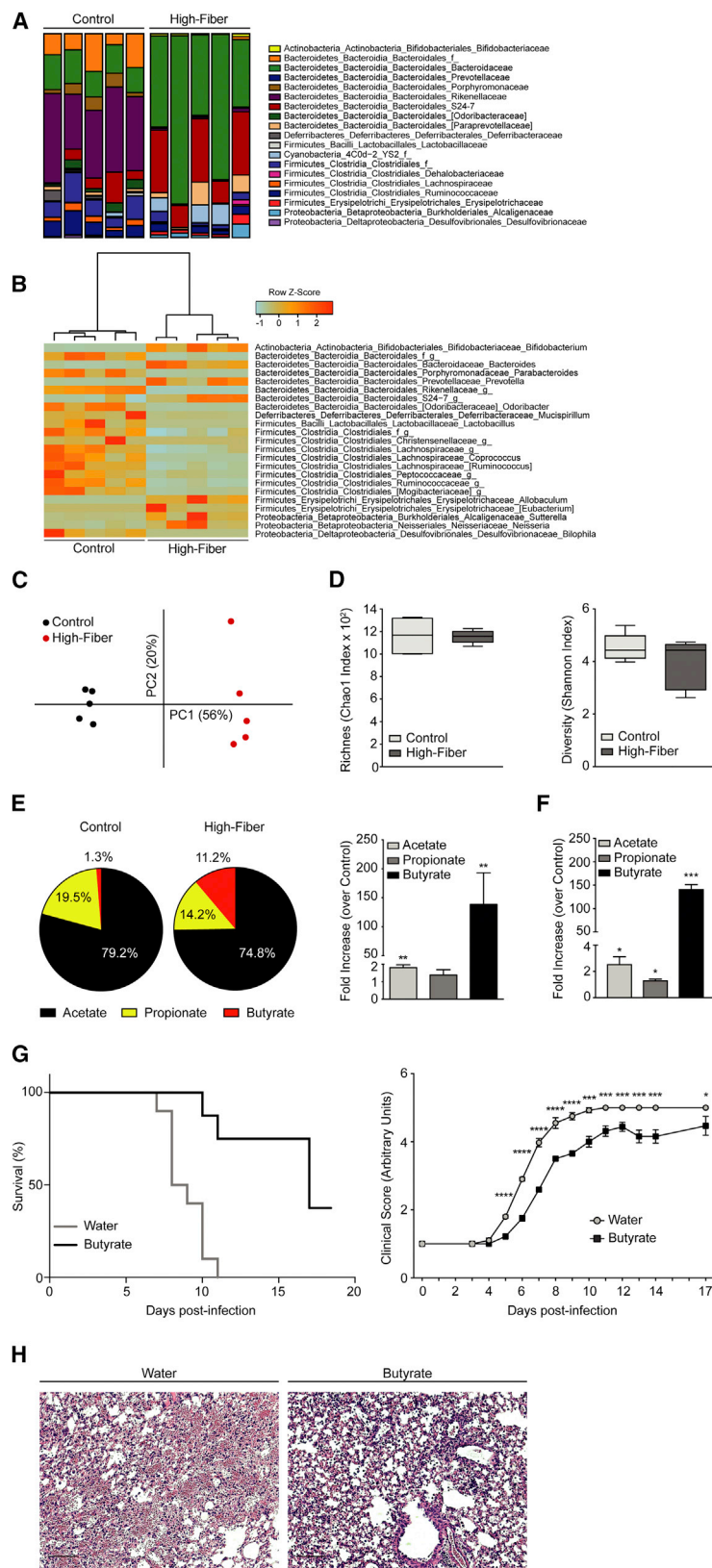


**Figure 2. Dietary Fiber Protects against Influenza-Induced Pathology by Altering Gut Microbial Composition and Short-Chain Fatty Acid (SCFA) Levels**

(A) Stacked bar plots showing the relative abundance of bacterial operational taxonomic units (OTUs) at family level for each individual of naive control or HFD-fed mice.

(B) Heatmap displaying main OTUs with significant differences in relative abundance among experimental groups with color-code representing row-scaled z-scores.

(C) Principal coordinates analysis (PCoA) based on Bray-Curtis dissimilarity matrix among all samples (ANOSIM  $R^2 = 0.27$ ,  $p = 0.00794$ ).

(D) Taxa richness (Chao1 index) and diversity (Shannon index) boxplots showing the median with min to max values.

(E) Composition of the three main SCFAs (acetate, propionate, and butyrate) in the feces of control and HFD-fed mice and their fold-increase over the control group in dry weight.

(F) Fold-increase of the three main SCFAs (acetate, propionate, and butyrate) in the serum of HFD-fed mice in comparison to the control group.

(G) Survival ( $p = 0.0002$ ) and clinical score of mice treated with butyrate during the course of high-dose infection.

(H) Representative H&E-stained lung tissue from control mice or mice receiving butyrate in drinking water on day 7 after high-dose infection. Scale bars, 100  $\mu\text{m}$ .

Results are representative of data generated in three independent experiments and are expressed as mean  $\pm$  SEM;  $n = 3-6$  per group in (A)-(F);  $n = 8-10$  per group in (G) and (H). Statistical significance was determined with Mantel-Cox test for the survival in (G) and with Student's t test (unpaired, two-tailed) in (E)-(G). \* $p = 0.05$ , \*\* $p = 0.01$ , \*\*\* $p = 0.001$ , \*\*\*\* $p = 0.0001$ .

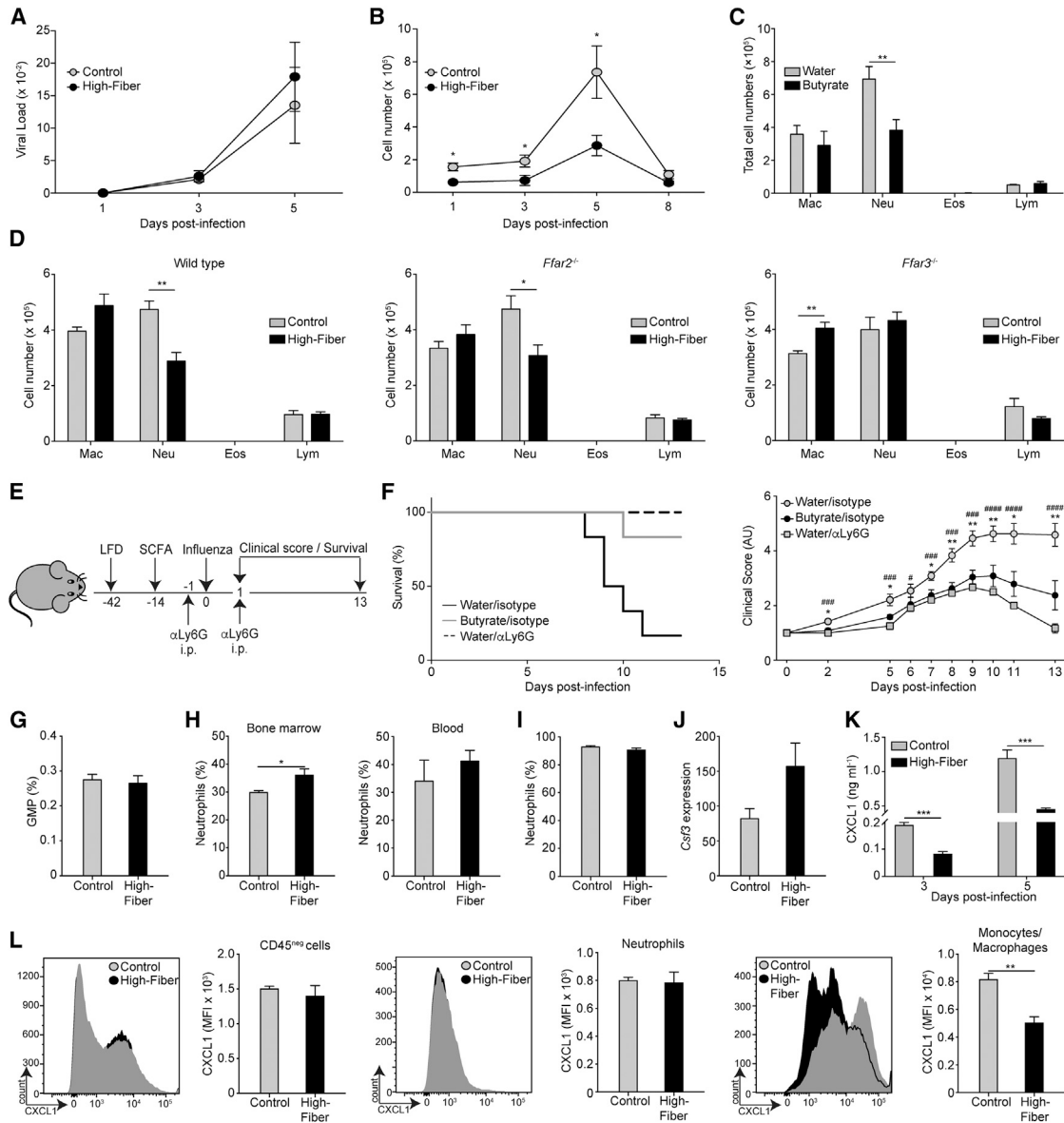


**Figure 3. Dietary Fiber Prevents Neutrophil Influx into the Airways in a SCFA- and FFAR3-Dependent Manner by Reducing Macrophage-Derived CXCL1 Production**

(A) Viral load in the lung of mice fed a control or HFD 1, 3, and 5 days after low-dose infection as measured by viral RNA expression in relation to  $\beta$ Actin.  
 (B) Neutrophil counts in the BALF of mice fed a control or HFD 1, 3, 5, and 8 days after low-dose infection as determined by differential cell counts.  
 (C) Differential cell counts in the BALF of mice treated with butyrate 5 days after low-dose infection. Mac, macrophages; Neu, neutrophils; Eos, eosinophils; Lym, lymphocytes.  
 (D) Differential cell counts in the BALF of wild-type, *Ffar2*<sup>-/-</sup>, and *Ffar3*<sup>-/-</sup> mice fed a control or HFD 5 days after infection. Mac, macrophages; Neu, neutrophils; Eos, eosinophils; Lym, lymphocytes.  
 (E) Experimental model of neutrophil reduction during high-dose infection in butyrate-treated animals.  
 (F) Survival ( $p = 0.0201$  for water/isotype versus butyrate/isotype;  $p = 0.0042$  for water/isotype versus water/ $\alpha$ Ly6G) and clinical score of neutrophil-reduced mice receiving either nothing or butyrate in drinking water.  
 (G) Frequency of granulocyte-macrophage progenitors (GMPs) in the bone marrow of control or HFD-fed mice 5 days after low-dose infection.  
 (H) Frequency of neutrophils in the bone marrow and in the blood of control or HFD-fed mice 5 days after low-dose infection.  
 (I) Frequency of neutrophils in the BALF of mice fed a control or HFD 6 hr after intranasal CXCL1 administration.  
 (J) mRNA expression of colony-stimulating factor 3 (*Csf3*) in the lung of mice fed a control or HFD 5 days after low-dose infection.  
 (K) Protein content of CXCL1 in the BALF of control or HFD-fed mice 3 and 5 days after low-dose infection.  
 (L) CXCL1 expression in the CD45<sup>-</sup> compartment, neutrophils, and monocytes/macrophages in control and HFD-fed animals 3 days after low-dose infection as determined by flow cytometry. MFI, mean fluorescence intensity.

(legend continued on next page)

had a normal neutrophil influx (Figure 3F). Survival and clinical score of neutrophil-attenuated animals were similar to those of butyrate-treated mice (Figure 3F), suggesting that the effect of butyrate on the clinical outcome of influenza infection was largely mediated by its ability to prevent excessive neutrophil recruitment into the airways. Thus, dietary fiber and SCFAs ameliorated the outcome of influenza infection and conveyed protection against immunopathology and tissue destruction by attenuating the neutrophil influx into the airways in a FFAR3-dependent manner.

The next step was to unravel how SCFAs lead to the reduced neutrophil influx seen in HFD-fed animals upon influenza infection. We have previously shown that dietary fiber can influence DC hematopoiesis via SCFAs (Trompette et al., 2014); hence, we determined whether granulopoiesis was similarly affected. The frequencies of the multipotent progenitor cells, common myeloid progenitors (Figure S1A), and that of the further differentiated granulocyte-macrophage progenitors (Figure 3G) were unaltered. Moreover, in the bone marrow, an increase in the proportion of mature neutrophils could be detected in HFD-fed compared to control diet-fed mice (Figure 3H). To address whether the decreased airway neutrophilia was due to the retention of neutrophils inside the bone marrow, we assessed the systemic levels of neutrophils. Neutrophil frequencies in the blood were equal between groups (Figure 3H), ruling out an impaired release into circulation. Reduced airway neutrophilia was also not due to an intrinsic defect of neutrophils to respond to their chemoattractant molecules via *Cxcr2*, as expression of this receptor was unaltered between control and HFD-fed mice (Figure S1B) and intranasal instillation of CXCL1, one of the major neutrophil-recruiting chemokines, led to equal neutrophil influx into the airways (Figure 3I). Moreover, levels of granulocyte colony-stimulating factor (*Csf3*), an important survival factor for neutrophils (Basu et al., 2002; Dienz et al., 2012), were not diminished in the lung of HFD-fed mice, indicating that there was no defect in this local neutrophil survival factor (Figure 3J). While the neutrophil-recruiting chemokines CCL3 and CXCL2 were not significantly different at 3 and 5 days after infection (Figure S1C), interleukin (IL)-1 $\beta$  and IL-6, which induce CXCL1 and CXCL2 expression (Biondo et al., 2014; Roy et al., 2012), were reduced in HFD-fed mice (Figure S1D). In line with this, we observed a marked reduction in CXCL1, the most abundant neutrophil chemoattractant in our model, in the airways of HFD-fed animals at both time points (Figure 3K). To elucidate which cell type is responsible for the blunted CXCL1 expression, intracellular staining of CXCL1 was performed in control and HFD-fed mice 3 days after infection. CD45<sup>+</sup> cells and neutrophils did not show any difference in CXCL1 expression between control and HFD-fed mice. However, the macrophage/monocyte compartment displayed a significant decrease in its ability to produce CXCL1 (Figure 3L). Similar results were obtained when butyrate was orally administered to mice (Figure S2).

### Dietary Fiber Reduces Airway Neutrophilia by Altering Hematopoiesis and Promoting the Differentiation of AAMs from Ly6c<sup>+</sup> Patrolling Monocytes

To address the functional difference seen in the lung macrophage population, we examined macrophage precursors in the bone marrow and found that macrophage-DC progenitors (MDPs) were increased in the bone marrow of HFD-fed animals (Figure 4A) 3 days after infection. Within the bone marrow, MDPs can give rise to monocytes and to common DC precursors (CDPs). No significant differences were observed in CDP frequencies between control and HFD-fed mice (data not shown), which pointed toward a potential effect on monocytes. In mice, two subsets of monocytes have been described, namely the Ly6c<sup>+</sup> (Gr-1<sup>+</sup>) inflammatory monocytes and the Ly6c<sup>+</sup> (Gr-1<sup>-</sup>) monocytes, the latter being referred to as patrolling monocytes (Fogg et al., 2006; Geissmann et al., 2010). Investigation of these monocyte subsets showed that this increase in precursor cells resulted in a markedly enhanced frequency of Ly6c<sup>+</sup> monocytes in the bone marrow (Figure 4B) and blood (Figure S3A), as well as in the lung of HFD-fed or SCFA-treated animals 3 days after infection (Figures 4C and S3B). Of note, the Ly6c<sup>+</sup> monocyte population remained unaltered in the bone marrow (Figure 4B) and in the lung (Figures 4C and S3B). Ly6c<sup>+</sup> patrolling monocytes have been shown to give rise to macrophages in the lung (Landsman and Jung, 2007; Landsman et al., 2007) and, upon tissue damage, these cells undergo a specific transcriptional program allowing them to differentiate into tissue repair AAMs (Auffray et al., 2007). In line with this, we found that interstitial as well as alveolar macrophages were increased in frequency when mice were fed a HFD (Figures 4D and 4E) or given butyrate orally (Figure S3C). Furthermore, these macrophages exhibited an alternative activation profile as determined by their surface expression of CD206 and programmed death-ligand (PD-L) 2 (Figures 4D and 4E). This finding was further supported by an increased mRNA expression of *Il-4* and *Il-10* in the lung of HFD-fed mice (Figure 4F), two cytokines known to promote alternative activation of macrophages (Wang et al., 2014), while the inflammatory macrophage-driving cytokine interferon (*ifn*)- $\gamma$  was unaltered (Figure 4G) 3 days after infection. To test whether dietary fiber can directly influence the differentiation of bone marrow cells into macrophages via SCFAs, bone marrow cells from control mice were differentiated into macrophages *ex vivo* for 7 days in the presence of different concentrations of butyrate and then subjected to their respective polarizing cytokines for 24 hr (Figure 4H). Administration of butyrate to the differentiation culture increased the number of cells that differentiated into macrophages after 7 days (Figure 4I), reflecting the observations made *in vivo*. Butyrate treatment during differentiation did not change the ratio between Arginase (*Arg*) 1 and Nitric oxide synthase (*Nos*) 2 at baseline (M0) or after addition of IFN- $\gamma$  (Figure 4J). However, the *Arg1/Nos2* ratio increased in a dose-dependent manner after IL-4 supplementation (M2)

Results are representative of data generated in at least two independent experiments and are expressed as mean  $\pm$  SEM; n = 3–6 per group and time point in (A) and (B); n = 5 per group in (C); n = 4–6 WT, n = 5–7 *Ffar2*<sup>-/-</sup>, n = 5 *Ffar3*<sup>-/-</sup> mice per group in (D); n = 6 per group in (F); n = 3–4 mice per group and time point in (G)–(L). Statistical significance was determined with Mantel-Cox test for the survival in (F) and with Student's t test (unpaired, two-tailed) in (A)–(L). \*p = 0.05, \*\*p = 0.01, \*\*\*p = 0.001, #p = 0.05, ###p = 0.001, ####p = 0.0001. \*for water/isotype versus butyrate/isotype, #for water/isotype versus water/ $\alpha$ Ly6G. See also Figures S1 and S2.

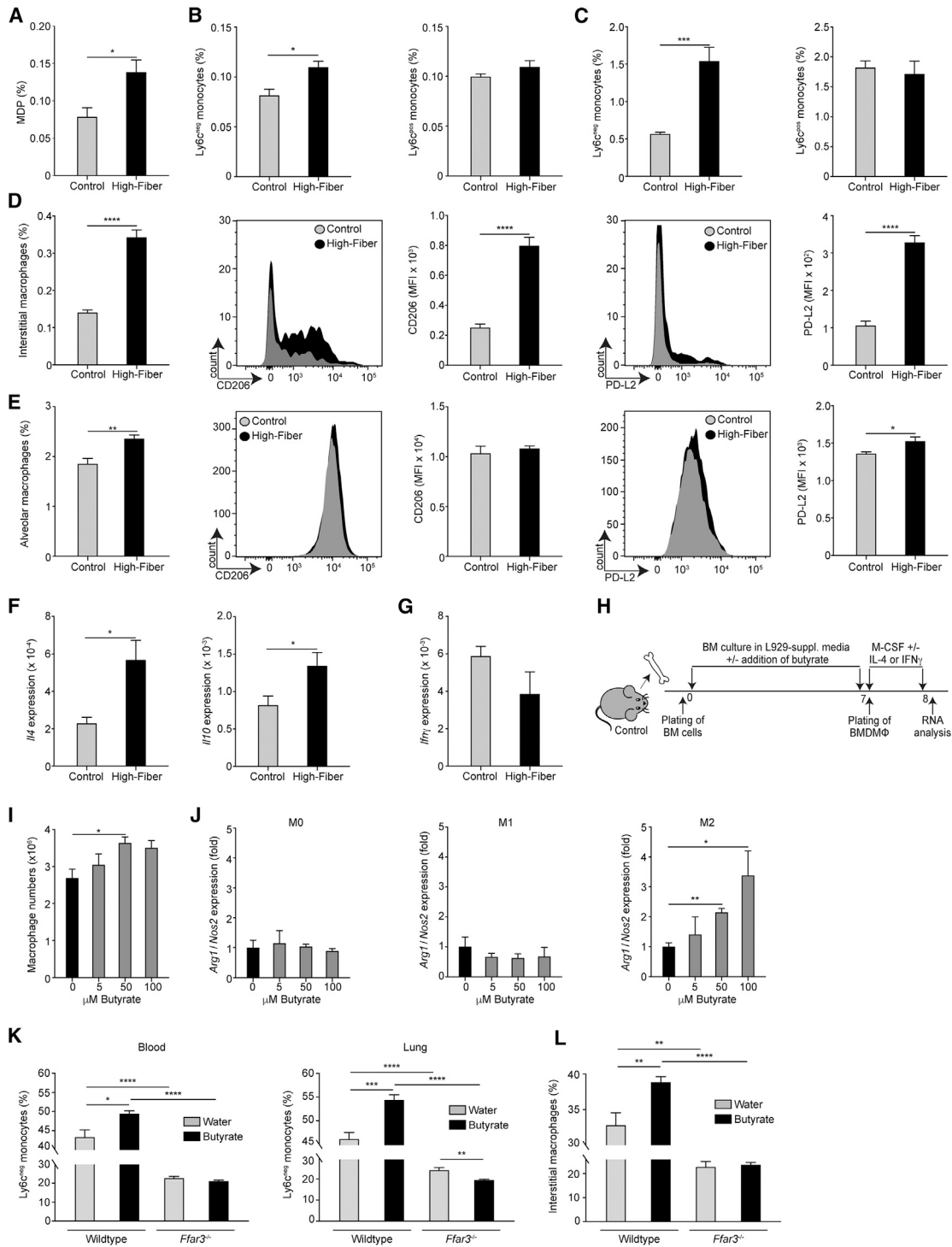


**Figure 4. Dietary Fiber Enhances Bone Marrow Hematopoiesis of Ly6c<sup>-</sup> Patrolling Monocytes, Leading to a Pulmonary Macrophage Population Enriched in Alternatively Activated Cells**

(A) Macrophage-dendritic cell progenitors (MDPs) in the bone marrow of control or HFD-fed mice 3 days after low-dose infection. (B and C) Frequencies of Ly6c<sup>-</sup> and Ly6c<sup>+</sup> monocytes in the bone marrow (B) and in the lung (C) of mice fed a control or HFD 3 days after low-dose infection. (D) Frequencies of interstitial macrophages and their surface expression of CD206 and PD-L2 in control and HFD-fed animals 3 days after low-dose infection. MFI, mean fluorescence intensity. (E) Frequencies of alveolar macrophages and their surface expression of CD206 and programmed death-ligand (PD-L) 2 in control and HFD-fed animals 3 days after low-dose infection. MFI, mean fluorescence intensity. (F) mRNA expression of interleukin (*Il*)-4 and *Il*-10 in the lung of mice fed a control or HFD 3 days after low-dose infection.

(legend continued on next page)

(Figure 4J), indicating that the presence of butyrate during bone marrow cell differentiation predisposes macrophages to develop an alternative activation profile upon appropriate cytokine stimulation. We previously showed that FFAR3 was required for the blunted neutrophilic response. To determine whether this outcome was due to a direct effect of SCFAs on macrophage precursors in the bone marrow and dependent on FFAR3, mixed wild-type and *Ffar3*<sup>-/-</sup> bone marrow chimeric animals were generated. The proportions of bone marrow-derived Ly6c<sup>-</sup> patrolling monocytes and interstitial macrophages present in the blood and lung of mice receiving butyrate or vehicle (water) orally were assessed 3 days after infection. We found that only the wild-type bone marrow compartment generated more patrolling monocytes, and subsequently, more interstitial macrophages, in response to butyrate (Figures 4K and 4L). Of note, patrolling monocytes and interstitial macrophages derived from *Ffar3*<sup>-/-</sup> bone marrow cells were also significantly less frequent in the water control group when compared to their wild-type counterparts (Figures 4K and 4L), pointing toward a critical role of FFAR3 for the SCFA-driven expansion of patrolling monocytes from bone marrow precursors. Taken together, our results showed that HFD shapes macrophage precursors in the bone marrow directly via SCFAs acting on FFAR3, which led to an elevated frequency of Ly6c<sup>-</sup> patrolling monocytes that were predisposed to differentiate into AAMs in the lung, a phenotype reinforced due to the increased presence of IL-4 and IL-10 in the lung of HFD-fed animals. It is well established that AAMs are less capable of producing the neutrophil chemoattractant CXCL1 (Labonte et al., 2014). The increased proportion of AAMs in the overall lung macrophage population of mice fed a HFD resulted in less CXCL1 being released and, hence, a blunted airway neutrophilia.

### Dietary Fiber Increases Anti-viral Immunity through CD8<sup>+</sup> T Cell Activation

To address whether adaptive anti-viral responses were also altered by dietary fiber, we assessed the CD8<sup>+</sup> T cell response during the course of infection in control and HFD-fed animals. Although total lymphocyte numbers (Figure S4A) and CD8<sup>+</sup> T cells in particular (Figure 5A) were unchanged 5 days after infection, CD8<sup>+</sup> T cells from HFD-fed mice were more activated, as represented by a higher frequency of cells expressing the degranulation marker CD107 $\alpha$  (Figure 5B). This CD8<sup>+</sup> T cell activation was unlikely to be due to DCs as the frequency and activation of CD11b<sup>+</sup> DCs (Figures S4B and S4C) and CD11b<sup>-</sup> DCs (Figures S4D and S4E) in the lung was unaltered or even diminished in HFD-fed animals at this time point. Later during infec-

tion (day 8), increased lymphocyte numbers could be found in the BALF of HFD-fed mice (Figure 5C). This was due to an expansion of CD8<sup>+</sup> T cells in the lung (Figure 5D), as CD4<sup>+</sup> T cell numbers remained unaltered (Figure S5A). The CD8<sup>+</sup> T cells exhibited lower expression of the lymph-node homing marker CD62L (Figure 5E) and we found a higher percentage of Granzyme B and CD107 $\alpha$ -expressing cells (Figure 5F), indicating increased tissue-homing and degranulation of CD8<sup>+</sup> T cells in HFD-fed animals. The percentage of influenza nuclear protein (NP)-specific CD8<sup>+</sup> T cells was elevated in the lung and BALF of HFD-fed mice (Figures 5G and S5B), so too were CD107 $\alpha$ -expressing NP-specific cells (Figure 5H); the anti-viral cytokine response was similarly augmented (Figures 5I and S5C). To test whether this enhanced activation state of CD8<sup>+</sup> T cells corresponded to an increased ability to kill virus-infected cells, we performed an *in vivo* killing assay. To this end, an equal amount of NP-pulsed and unpulsed CFSE-labeled splenocytes were injected into influenza-infected control and HFD mice 7 days after infection and the proportion of live NP-pulsed cells was determined 14 hr later. HFD-fed animals eliminated more NP-pulsed cells than control animals (Figure 5J), indicating that the enhanced activation state of CD8<sup>+</sup> T cells translated into a higher cytotoxic capacity. This also corresponded with an accelerated clearance of the virus (Figure 5K). At this later time point, the enhanced CD8<sup>+</sup> T cell cytotoxic activity was still not associated with an increased DC response (Figures S5D and S5E), indicative of an intrinsic CD8<sup>+</sup> T cell phenomenon. To test whether dietary fiber could augment effector function via a direct effect of SCFAs on CD8<sup>+</sup> T cells, CD8<sup>+</sup> T cells from control mice were isolated and cultured in the presence of increasing concentrations of butyrate. Addition of butyrate decreased the proportion of CD62L<sup>+</sup> cells and increased the frequency of CD107 $\alpha$ <sup>+</sup> lymphocytes (Figure 5L), indicating a direct influence of SCFAs upon CD8<sup>+</sup> T cell activation. To test these findings, we next investigated whether the effects of HFD and SCFAs upon CD8<sup>+</sup> T cell effector function were intrinsic to T cells and mediated via FFAR3. By co-transferring CD8<sup>+</sup> T cells from wild-type and *Ffar3*<sup>-/-</sup> into *Cd8*<sup>-/-</sup> recipient animals administered butyrate, we found that only CD8<sup>+</sup> T cells from wild-type mice had the capacity to expand upon butyrate supplementation, as demonstrated by a higher percentage of influenza-specific CD8<sup>+</sup> T cells in the lung 8 days after infection (Figures 5M). CD8<sup>+</sup> T cells from wild-type mice also increased the expression of CD107 $\alpha$  and their anti-viral cytokine response upon butyrate treatment, something that the CD8<sup>+</sup> T cells from *Ffar3*<sup>-/-</sup> failed to achieve (Figures 5N). Of note, influenza-specific CD8<sup>+</sup> T cells derived from *Ffar3*<sup>-/-</sup>

(G) mRNA expression of interferon (*Ifr*)- $\gamma$  in the lung of mice fed a control or HFD 3 days after low-dose infection.

(H) Experimental model for the differentiation and polarization of bone marrow-derived macrophages in the presence of butyrate.

(I) Macrophage numbers 7 days after differentiation with 10% L929 supernatant in the presence or absence of butyrate.

(J) Fold-change of the ratio between Arginase (*Arg*) 1 and inducible nitric oxid synthase (*Nos2*) mRNA expression before polarization (M0) and after 24 hr of M1 or M2 polarization.

(K) Frequencies of Ly6c<sup>-</sup> monocytes derived from wild-type (*Ly5.1*) and *Ffar3*<sup>-/-</sup> (*Ly5.2*) bone marrow donor cells in the blood and lung of lethally irradiated wild-type recipient mice administered water or butyrate 3 days after a low-dose infection.

(L) Frequencies of interstitial macrophages derived from wild-type (*Ly5.1*) and *Ffar3*<sup>-/-</sup> (*Ly5.2*) bone marrow donor cells in the lung of lethally irradiated wild-type recipient mice administered water or butyrate 3 days after a low-dose infection.

Results are representative of data generated in at least two independent experiments and are expressed as mean  $\pm$  SEM. Bone marrow *in vitro* data in (I) and (J) are pooled from three independent experiments.  $n = 3-5$  mice per group in (A)-(G);  $n = 6-7$  mice per group in (K) and (L). Statistical significance was determined with Student's *t* test (unpaired, two-tailed). \* $p = 0.05$ , \*\* $p = 0.01$ , \*\*\* $p = 0.001$ , \*\*\*\* $p = 0.0001$ . See also Figure S3.

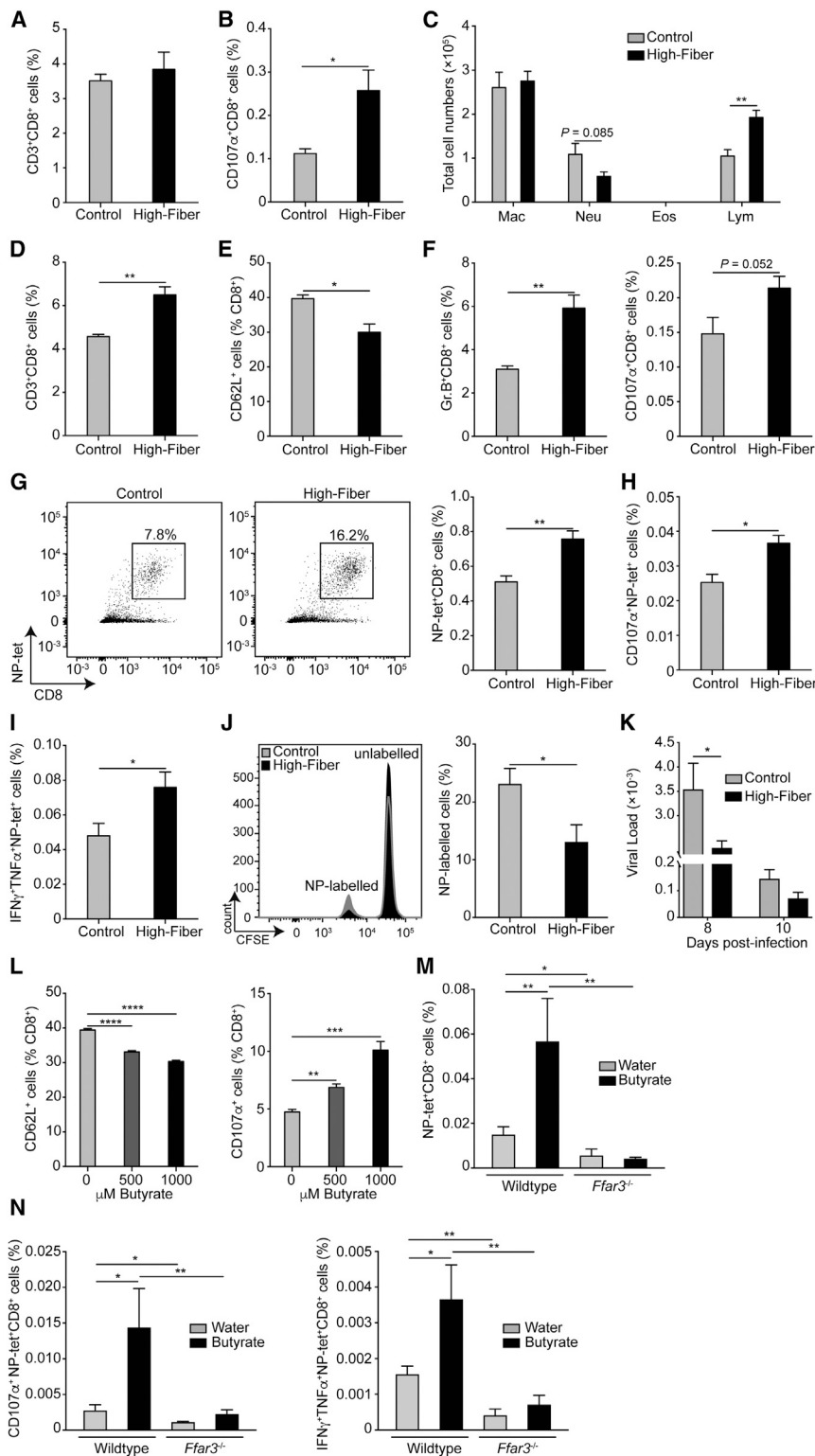


**Figure 5. Dietary Fiber Boosts Anti-viral CD8<sup>+</sup> T Cell Responses**

(A) Frequency of CD8<sup>+</sup> T cells in the lung of control or HFD-fed mice 5 days after low-dose infection. (B) Frequency of CD107 $\alpha$ -expressing CD8<sup>+</sup> T cells in the lung of mice fed a control or HFD 5 days after low-dose infection.

(C) Differential cell counts in the BALF of mice fed a control or HFD 8 days after low-dose infection. Mac, macrophages; Neu, neutrophils; Eos, eosinophils; Lym, lymphocytes.

(D) Frequency of CD8<sup>+</sup> T cells in the lung of control or HFD-fed mice 8 days after low-dose infection.

(E and F) Frequency of CD62L-expressing (E) and granzyme (Gr.) B-producing and CD107 $\alpha$ -expressing (F) CD8<sup>+</sup> T cells in the lung of control or HFD-fed mice 8 days after low-dose infection.

(G) Frequency of influenza nuclear protein (NP)-positive CD8<sup>+</sup> T cells in the lung of control or HFD-fed mice 8 days after low-dose infection.

(H) Frequency of CD107 $\alpha$ -expressing influenza-specific NP<sup>+</sup>CD8<sup>+</sup> T cells in the lung of control or HFD-fed mice 8 days after low-dose infection.

(I) Frequency of IFN- $\gamma$  and tumor necrosis factor (TNF)  $\alpha$  double-producing influenza-specific NP<sup>+</sup>CD8<sup>+</sup> T cells in the lung of control or HFD-fed mice 8 days after low-dose infection.

(J) Proportion of live NP-labeled CFSE<sup>lo</sup> splenocytes injected 7 days after low-dose infection in control or HFD-fed mice as determined by flow cytometry 14 hr post-injection.

(K) Viral load in the lung of mice fed a control or HFD 8 and 10 days after low-dose infection.

(L) Frequency of CD62L and CD107 $\alpha$ -expressing cells after 24 hr *in vitro* activation of naive CD8<sup>+</sup> T cells isolated from the spleen of control mice in the presence or absence of butyrate.

(M and N) Frequencies of influenza-specific NP<sup>+</sup>CD8<sup>+</sup> T cells (M), as well as CD107 $\alpha$ -expressing NP<sup>+</sup>CD8<sup>+</sup> T cells and IFN- $\gamma$ /TNF- $\alpha$  double-producing NP<sup>+</sup>CD8<sup>+</sup> T cells (N) from wild-type (*Ly5.1*) and *Ffar3*<sup>-/-</sup> (*Ly5.2*) donors present in the lung of *Cd8*<sup>-/-</sup> recipient mice administered water or butyrate 8 days after low-dose infection.

Results are representative of data generated in two to three independent experiments and are expressed as mean  $\pm$  SEM; n = 4–5 per group and time point (A)–(L); n = 4 in (K); n = 6–8 in (M). Statistical significance was determined with Student's t test (unpaired, two-tailed). \*p = 0.05, \*\*p = 0.01, \*\*\*p = 0.001, \*\*\*\*p = 0.0001. See also Figures S4 and S5.

### Dietary Fiber Enhances Adaptive Immunity by Altering CD8<sup>+</sup> T Cell Metabolism

To test whether the altered activation of CD8<sup>+</sup> T cells in HFD-fed mice was linked to a change in cellular metabolism, we

isolated CD8<sup>+</sup> T cells from control and HFD-fed animals and screened their metabolic profile. Naive CD8<sup>+</sup> T cells from HFD-fed mice exhibited elevated concentrations of most of the metabolites analyzed, notably those of the tricarboxylic acid (TCA) cycle (Figure 6A). CD8<sup>+</sup> T cells isolated from naive control

donors were also significantly less frequent and functional in the water control group when compared to their wild-type counterparts, underlining the critical role of FFAR3 for the expansion and functionality of influenza-specific CD8<sup>+</sup> T cells in response to SCFAs.

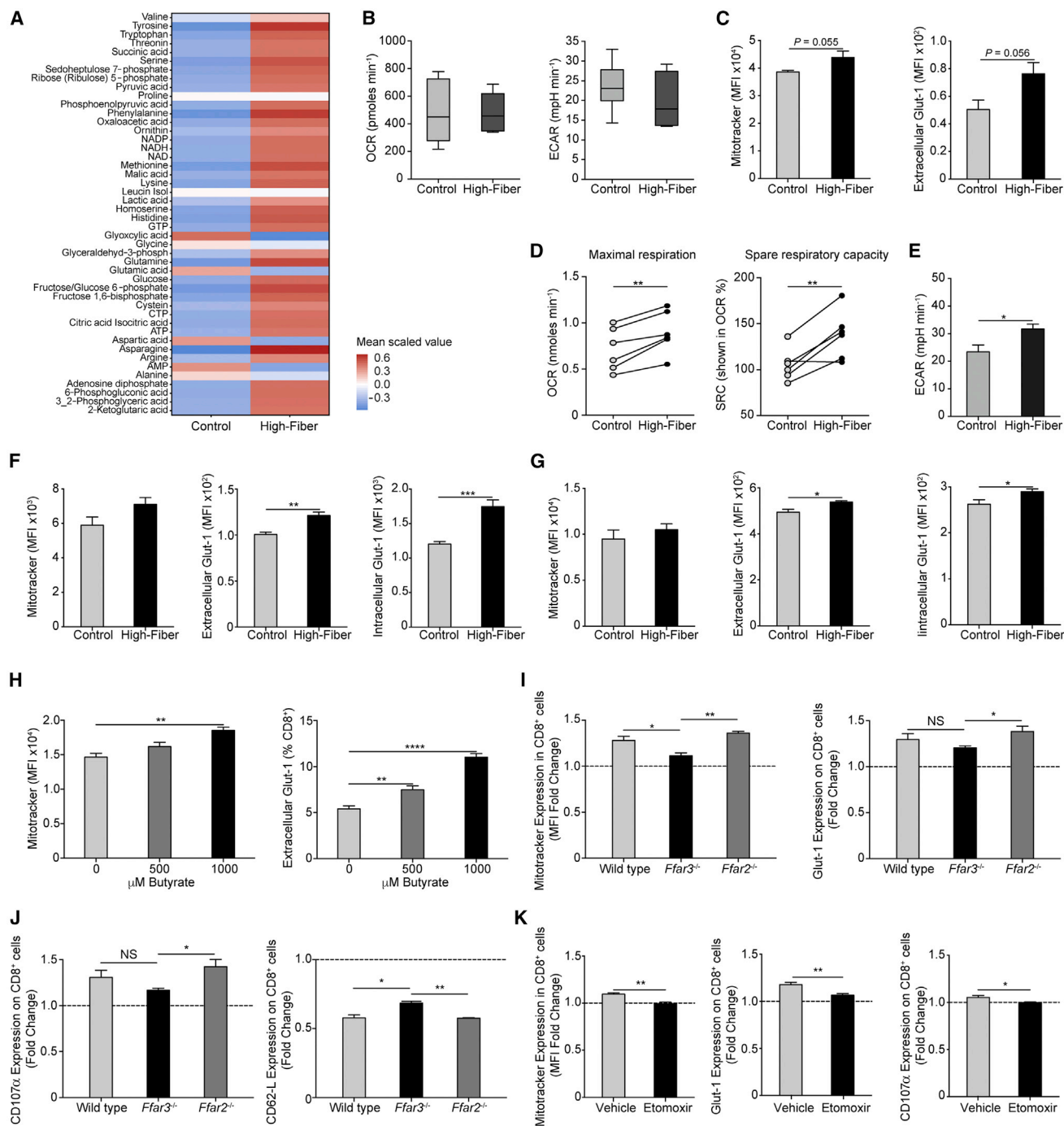


**Figure 6. Dietary Fiber Influences CD8<sup>+</sup> T Cell Metabolism via FFAR3 and Fatty Acid Oxidation (FAO)**

(A) Heatmap depicting an absolute metabolic quantification analyzed by LC-tandem mass spectrometry.  
 (B) Basal oxygen consumption rate (OCR) and extracellular acidification rate (ECAR) of naive splenic CD8<sup>+</sup> T cells isolated from control and HFD-fed mice.  
 (C) Mitochondrial mass as measured by mitotracker staining and surface Glut-1 expression on naive pulmonary CD8<sup>+</sup> T cells from control or HFD-fed mice. MFI, mean fluorescence intensity.  
 (D) Maximal respiration and spare respiratory capacity (measured in OCR after carbonyl cyanide-p-trifluoromethoxyphenylhydrazone [FCCP] addition) of shortly activated CD8<sup>+</sup> T cells from control and HFD-fed mice.  
 (E) Glycolytic capacity of shortly-activated CD8<sup>+</sup> T cells from control and HFD-fed mice as measured after starvation and subsequent addition of glucose.  
 (F) Mitochondrial mass as measured by mitotracker staining as well as surface and intracellular Glut-1 expression on pulmonary CD8<sup>+</sup> T cells from control or HFD-fed mice 5 days after low-dose infection. MFI, mean fluorescence intensity.  
 (G) Mitochondrial mass as measured by mitotracker staining as well as surface and intracellular Glut-1 expression on pulmonary CD8<sup>+</sup> T cells from control or HFD-fed mice 8 days after low-dose infection. MFI, mean fluorescence intensity.

(legend continued on next page)

and HFD-fed mice exhibited similar basal oxygen consumption rates (OCR) and extracellular acidification rates (ECAR), measures of oxidative mitochondrial respiration and glycolytic function, respectively (Figure 6B). Similarly, only minor differences in mitochondrial mass and surface expression of the main glucose transporter in T cells, Glut-1 (Palmer et al., 2015), were observed in naive CD8<sup>+</sup> T cells (Figure 6C). However, maximal respiration and spare respiratory capacity of CD8<sup>+</sup> T cells from HFD-fed mice were significantly increased after a short period of *in vitro* stimulation (Figure 6D), as was the mitochondrial mass (Figure S6A), reflective of an enhanced potential to perform mitochondrial respiration. Their glycolytic capacity, as tested after glucose deprivation, was also increased (Figure 6E), suggesting an enhanced capacity to rely on anaerobic glycolysis. Extra- and intracellular levels of Glut-1 and *c-myc*, well-described inducers of glycolysis (Osthus et al., 2000; Palmer et al., 2015), were more potently increased upon stimulation of CD8<sup>+</sup> T cells isolated from HFD-fed mice (Figure S6B). This immediate metabolic boost correlated with a more activated phenotype of CD8<sup>+</sup> T cells from HFD-fed animals as shown by an increased frequency of CD107 $\alpha$ <sup>+</sup> and decreased percentage of CD62L<sup>+</sup> cells (Figure S6C). A similar phenotype could be observed in pulmonary CD8<sup>+</sup> T cells 5 days after influenza infection (Figures 6F and S6D), while by 8 days after infection, metabolic differences had diminished (Figures 6G and S6E). However, the increased activation state of CD8<sup>+</sup> T cells from HFD-fed animals persisted through to this time point (Figures 5E and 5F). The metabolic changes observed in HFD-fed mice could be attributed to a direct effect of butyrate on the CD8<sup>+</sup> T cells, as addition of butyrate to *in vitro*-stimulated CD8<sup>+</sup> T cells increased mitochondrial mass and surface Glut-1 expression in a dose-dependent manner (Figure 6H). SCFAs have been shown to induce metabolic changes in cells in several ways, including via GPR interactions (Blad et al., 2012; den Besten et al., 2013). We found that CD8<sup>+</sup> T cells express low levels of both FFAR3 and FFAR2 (data not shown). Addition of butyrate to CD8<sup>+</sup> T cells isolated from control diet-fed wild-type, *Ffar3*<sup>-/-</sup>, and *Ffar2*<sup>-/-</sup> mice revealed that the increase in mitochondrial mass and surface Glut-1 expression was partially dependent on FFAR3 (Figure 6I), which resulted in a less activated phenotype (Figure 6J). In addition, SCFAs can directly influence cellular metabolism by acting as substrates for FAO (Donohoe et al., 2011). To test whether this characteristic accounts for the FFAR3-independent increase in metabolic function and cell activation, etomoxir, an inhibitor of Carnitine palmitoyltransferase 1 (CPT1)-dependent FAO, was added to a culture of wild-type CD8<sup>+</sup> T cells. Etomoxir prevented

increased mitochondrial mass, surface levels of Glut-1, and CD107 $\alpha$  expression in response to butyrate (Figure 6K). Thus, dietary fiber and SCFAs enhanced CD8<sup>+</sup> T cell-intrinsic anti-viral responses through alterations of their cellular metabolism by serving as a substrate for FAO and by specifically interacting with FFAR3.

## DISCUSSION

The beneficial effect of dietary fiber and SCFAs in dampening chronic inflammatory disorders, such as allergies (Maslowski et al., 2009; Trompette et al., 2014), has received substantial attention and supported momentum toward their use in clinical studies. However, little is known about the effects of dietary fiber and SCFAs on protective immunity against infections—a clear concern when considering their clinical use. In this study, we report that dietary fiber and SCFAs have dual beneficial effects on the immune system that allow mice to control influenza infections more effectively. This involves both dampening and enhancing discrete components of the immune system such that the immunological tone in the airways is set at a level that allows viral clearance but avoids exaggerated tissue damage.

Tissue destruction due to uncontrolled innate immune responses upon influenza virus infection can result in severe morbidity and mortality (Damjanovic et al., 2012), an observation that we also made in our control mice. By reducing the influx of neutrophils into the airways in an indirect manner, dietary fiber and butyrate prevented immunopathology and alveolar hemorrhage. This was achieved by a mechanism involving a gut-bone marrow-lung axis similar to what we previously described for asthma (Trompette et al., 2014). In the context of allergic airway inflammation, bone marrow-derived DCs were altered and were key players for the dampened immune response (Trompette et al., 2014); however, in the context of infection there is a selective increase in Ly6c<sup>-</sup> patrolling monocytes that give rise to AAMs in the lung. Thus, the effect of dietary fiber and SCFAs on bone marrow hematopoiesis seems largely context dependent.

Macrophage-DC progenitors in the bone marrow give rise to common DC precursors and two subsets of monocytes: Ly6c<sup>+</sup> (Gr-1<sup>+</sup>) inflammatory monocytes and Ly6c<sup>-</sup> (Gr-1<sup>-</sup>) patrolling monocytes (Fogg et al., 2006; Geissmann et al., 2010). Ly6c<sup>+</sup> inflammatory monocytes can further differentiate into inflammatory DCs or macrophages (Geissmann et al., 2010) and have been shown to promote tissue damage during influenza infection (Aldridge et al., 2009). The Ly6c<sup>-</sup> patrolling monocytes have

(H) Mitochondrial mass as measured by mitotracker staining and frequency of cells expressing Glut-1 on the surface after 24 hr *in vitro* activation of naive CD8<sup>+</sup> T cells isolated from the spleen of control mice in the presence or absence of butyrate. MFI, mean fluorescence intensity.

(I) Fold-change in mitochondrial mass as measured by mitotracker staining and surface Glut-1 expression after 24 hr *in vitro* activation of naive CD8<sup>+</sup> T cells isolated from the spleen of wild-type, *Ffar3*<sup>-/-</sup>, and *Ffar2*<sup>-/-</sup> mice in the presence of 500  $\mu$ M butyrate as compared to the control media.

(J) Fold-change in CD107 $\alpha$  and CD62L expression after 24 hr *in vitro* activation of naive CD8<sup>+</sup> T cells isolated from the spleen of wild-type, *Ffar3*<sup>-/-</sup>, and *Ffar2*<sup>-/-</sup> mice in the presence of 500  $\mu$ M butyrate as compared to the control media.

(K) Fold-change in mitochondrial mass as measured by mitotracker staining, surface Glut-1, and CD107 $\alpha$  expression after 24 hr *in vitro* activation of naive CD8<sup>+</sup> T cells in the presence of 500  $\mu$ M butyrate as compared to the control media. 500  $\mu$ M etomoxir was added throughout the whole culture period to block fatty acid oxidation.

Results in (C) and (E)–(K) are representative of data generated in two to three independent experiments; results in (B) and (D) are pooled from six individual experiments. All results are expressed as mean  $\pm$  SEM; n = 3–6 per group in (A), (C), (E)–(G); n = 6 per group in (B) and (D); n = 4 in (H); n = 3 in (I)–(K). Statistical significance was determined with Student's t test (unpaired, two-tailed in A–C and E–K; paired in D). NS, not significant; \*p = 0.05, \*\*p = 0.01, \*\*\*p = 0.001, \*\*\*\*p = 0.0001. See also Figure S6.

been described to generate AAMs (Auffray et al., 2009), which are known to contribute to tissue protection and repair upon inflammation and infection (Auffray et al., 2007; Nahrendorf et al., 2007). In the context of respiratory syncytial virus infection, AAMs have been shown to be important in the resolution of virus-induced lung injury (Shirey et al., 2010). Moreover, AAMs are less capable of producing neutrophil-attracting chemokines such as CXCL1 (Labonte et al., 2014), thereby preventing the accumulation of cytotoxic neutrophils inside the airways. In our study, we show that these cells are playing a pivotal role in the protection against influenza-induced immunopathology. Dietary fiber and SCFAs, by acting on FFAR3, specifically increase the frequency of Ly6c<sup>-</sup> patrolling monocytes being released from the bone marrow and infiltrating the lung upon infection. Once within the lung microenvironment, these cells differentiate into AAMs. It should be noted that the term AAM broadly refers to macrophages with an M2 phenotype, and given the plasticity of macrophage gene expression, this term is convenient but an oversimplification. It is most relevant to refer to the lung macrophages by their function, which in the current study we found is to prevent overshooting neutrophil recruitment and, hence, decrease tissue damage and hemorrhage following influenza infection.

Although Ly6c<sup>+</sup> inflammatory monocytes are known to induce immunopathology during influenza infection, they have also been reported to be important for viral clearance by priming virus-specific CD8<sup>+</sup> T cells (Aldridge et al., 2009). It is noteworthy that the increase in Ly6c<sup>-</sup> patrolling monocytes did not result in a reduction of the Ly6c<sup>+</sup> inflammatory monocyte subset and, therefore, did not inhibit necessary anti-viral responses. This is further underlined by the increased virus-specific CD8<sup>+</sup> T cell response we observed.

Our data show that dietary fiber can alter CD8<sup>+</sup> T cell metabolism to accelerate and enhance effector function. Immediately upon stimulation, previously naive CD8<sup>+</sup> T cells from HFD-fed mice exhibit increased mitochondrial mass and elevated maximal respiration and spare respiratory capacity, an overall indicator of an enhanced capability to use oxidative phosphorylation (OXPHOS). At the same time, their glycolytic capacity is augmented. Naive T cells largely rely on the OXPHOS pathway to produce energy (Buck et al., 2015; O'Sullivan and Pearce, 2015). During effector cell differentiation, cellular metabolism gets switched to glycolysis to guarantee the production of metabolic intermediates important for cell growth and proliferation (Buck et al., 2015; O'Sullivan and Pearce, 2015). The effector phase is finally marked by a concomitant high glycolytic rate and OXPHOS activity (Buck et al., 2015; O'Sullivan and Pearce, 2015), something we see after short-term activation of CD8<sup>+</sup> T cells from HFD-fed animals, indicating that dietary fiber promotes immediate effector cell differentiation and activation by influencing cellular metabolism similar to what can also be seen during memory recall responses. Moreover, effector cells from HFD-fed mice show increased functionality. The functional capacity of CD8<sup>+</sup> T cells is largely dependent on glucose availability and uptake (Cham et al., 2008; Jacobs et al., 2008). Glut-1, the main glucose transporter in T cells (Palmer et al., 2015), translocates to the cell surface upon activation to allow glucose uptake (Wieman et al., 2007). HFD-fed mice displayed increased surface expression of Glut-1, allowing enhanced glucose assimilation. Moreover, the intracellular pool of Glut-1

was also elevated in these mice, providing a bigger reservoir of transporters. This is in line with the increased activation state of CD8<sup>+</sup> T cells from HFD-fed mice.

The metabolic and functional changes in CD8<sup>+</sup> T cells are in part mediated by SCFAs through FFAR3. The mechanism by which FFAR3 can influence cellular metabolism is still unknown. One possibility could be the activation of extracellular signal-regulated kinase (ERK), which has been shown to induce glucose uptake and glycolysis in T cells (Marko et al., 2010). However, butyrate does not rely solely on FFAR3 to alter the cellular metabolism of CD8<sup>+</sup> T cells in HFD-fed mice. Etomoxir, a chemical compound inhibiting FAO by blocking the import of fatty acids into the mitochondria, also reverts the metabolic and functional changes induced by butyrate exposure of CD8<sup>+</sup> T cells. In addition to their capacity to induce GPR signaling and inhibit histone deacetylases, SCFAs such as butyrate can also directly enter cells and serve as a substrate for FAO (Blad et al., 2012; den Besten et al., 2013). Acetyl-CoA produced during FAO can then fuel the OXPHOS and glycolytic pathways (Kim et al., 2016; Nsiah-Sefaa and McKenzie, 2016; van der Windt et al., 2012). Thus, dietary fiber and SCFAs can alter CD8<sup>+</sup> T cell metabolism in multiple ways to ensure rapid and sustained activation of effector T cells upon viral infection. This finding is in line with a recent study which shows that increased endogenous serum acetate concentrations after systemic bacterial infection induce rapid CD8<sup>+</sup> memory T cell recall responses by shifting their cellular metabolism toward glycolysis (Balmer et al., 2016).

In summary, our data demonstrate that dietary fiber and SCFAs can protect against severe influenza infection by reducing tissue damage and by boosting adaptive anti-viral immunity. SCFAs have predominantly been associated with immunoregulation and the prevention of exaggerated inflammation (Maslowski et al., 2009; Trompette et al., 2014); however, our work highlights a dual role of SCFAs. By tuning down excessive innate responses, promoting tissue-protective mechanisms, and stimulating specific adaptive immunity, dietary fiber and SCFAs can create an immune balance that ultimately protects against disease.

## STAR★METHODS

Detailed methods are provided in the online version of this paper and include the following:

- **KEY RESOURCES TABLE**
- **CONTACT FOR REAGENT AND RESOURCE SHARING**
- **EXPERIMENTAL MODEL AND SUBJECT DETAILS**
  - Experimental Animals
  - Rodent Diets
  - SCFA Treatment
  - Animal Model of Influenza A Infection
  - *In Vitro* Bone Marrow Differentiation Cultures
  - Bone Marrow Macrophage Polarization
- **METHOD DETAILS**
  - Cellular Infiltration of the Airways
  - Measurement of Lung Function
  - Histology
  - ELISAs
  - *In vivo* Neutrophil Reduction

- *In vivo* Neutrophil Chemoattraction Assay
- *In Vivo* Killing Assay
- Flow Cytometry
- Metabolite screening
- SCFA Quantification
- Bacterial DNA Isolation from Mouse Feces
- 16S rRNA Library Preparation and Sequencing
- 16S rRNA Gene Sequencing Data Analysis
- Quantitative Polymerase Chain Reaction (qPCR)
- CD8<sup>+</sup> T Cell Adoptive Transfer
- Mixed Bone Marrow Chimeras
- *In Vitro* CD8<sup>+</sup> T Cell Assays
- CD8<sup>+</sup> T Cell Metabolic Assays
- **QUANTIFICATION AND STATISTICAL ANALYSIS**

### SUPPLEMENTAL INFORMATION

Supplemental Information includes six figures and one table and can be found with this article online at <https://doi.org/10.1016/j.immuni.2018.04.022>.

### ACKNOWLEDGMENTS

We are grateful to Norbert Sprenger, Christine Martin-Paschoud, and Catherine Murset-Mounoud for assistance with the SCFA quantification and to Alexis Rapin for sequencing support. This work was supported by an SNF grant 310030\_166210 awarded to B.J.M.

### AUTHOR CONTRIBUTIONS

B.J.M., A.T., and E.S.G. designed the study. A.T., E.S.G., C.P., N.U., E.R., I.C.L.-M., and J.P. performed experiments. A.T., E.S.G., C.P., and I.C.L.-M. analyzed data. L.P.N, L.F., E.S.G., A.T., and B.J.M. provided critical analysis and discussions. A.T., E.S.G., and B.J.M. wrote the paper.

### DECLARATION OF INTERESTS

The authors declare no competing interests.

Received: June 15, 2017

Revised: February 8, 2018

Accepted: April 19, 2018

Published: May 15, 2018

### REFERENCES

- Aldridge, J.R., Jr., Moseley, C.E., Boltz, D.A., Negovetich, N.J., Reynolds, C., Franks, J., Brown, S.A., Doherty, P.C., Webster, R.G., and Thomas, P.G. (2009). TNF/INOS-producing dendritic cells are the necessary evil of lethal influenza virus infection. *Proc. Natl. Acad. Sci. USA* *106*, 5306–5311.
- Aoyama, M., Kotani, J., and Usami, M. (2010). Butyrate and propionate induced activated or non-activated neutrophil apoptosis via HDAC inhibitor activity but without activating GPR-41/GPR-43 pathways. *Nutrition* *26*, 653–661.
- Arpaia, N., Campbell, C., Fan, X., Dikiy, S., van der Veecken, J., deRoos, P., Liu, H., Cross, J.R., Pfeiffer, K., Coffey, P.J., and Rudensky, A.Y. (2013). Metabolites produced by commensal bacteria promote peripheral regulatory T-cell generation. *Nature* *504*, 451–455.
- Auffray, C., Fogg, D., Garfa, M., Elain, G., Join-Lambert, O., Kayal, S., Sarnacki, S., Cumanan, A., Lauvau, G., and Geissmann, F. (2007). Monitoring of blood vessels and tissues by a population of monocytes with patrolling behavior. *Science* *317*, 666–670.
- Auffray, C., Sieweke, M.H., and Geissmann, F. (2009). Blood monocytes: development, heterogeneity, and relationship with dendritic cells. *Annu. Rev. Immunol.* *27*, 669–692.
- Balmer, M.L., Ma, E.H., Bantug, G.R., Grählert, J., Pfister, S., Glatzer, T., Jauch, A., Dimeloe, S., Slack, E., Dehio, P., et al. (2016). Memory CD8(+) T cells require increased concentrations of acetate induced by stress for optimal function. *Immunity* *44*, 1312–1324.
- Basu, S., Hodgson, G., Katz, M., and Dunn, A.R. (2002). Evaluation of role of G-CSF in the production, survival, and release of neutrophils from bone marrow into circulation. *Blood* *100*, 854–861.
- Biondo, C., Mancuso, G., Midiri, A., Signorino, G., Domina, M., Lanza Cariccio, V., Mohammadi, N., Venza, M., Venza, I., Teti, G., and Beninati, C. (2014). The interleukin-1 $\beta$ /CXCL1/2/neutrophil axis mediates host protection against group B streptococcal infection. *Infect. Immun.* *82*, 4508–4517.
- Blad, C.C., Tang, C., and Offermanns, S. (2012). G protein-coupled receptors for energy metabolites as new therapeutic targets. *Nat. Rev. Drug Discov.* *11*, 603–619.
- Brandes, M., Klauschen, F., Kuchen, S., and Germain, R.N. (2013). A systems analysis identifies a feedforward inflammatory circuit leading to lethal influenza infection. *Cell* *154*, 197–212.
- Buck, M.D., O'Sullivan, D., and Pearce, E.L. (2015). T cell metabolism drives immunity. *J. Exp. Med.* *212*, 1345–1360.
- Caporaso, J.G., Kuczynski, J., Stombaugh, J., Bittinger, K., Bushman, F.D., Costello, E.K., Fierer, N., Peña, A.G., Goodrich, J.K., Gordon, J.I., et al. (2010). QIIME allows analysis of high-throughput community sequencing data. *Nat. Methods* *7*, 335–336.
- Carmody, R.N., Gerber, G.K., Luevano, J.M., Jr., Gatti, D.M., Somes, L., Svenson, K.L., and Turnbaugh, P.J. (2015). Diet dominates host genotype in shaping the murine gut microbiota. *Cell Host Microbe* *17*, 72–84.
- Cham, C.M., Driessens, G., O'Keefe, J.P., and Gajewski, T.F. (2008). Glucose deprivation inhibits multiple key gene expression events and effector functions in CD8<sup>+</sup> T cells. *Eur. J. Immunol.* *38*, 2438–2450.
- Chang, P.V., Hao, L., Offermanns, S., and Medzhitov, R. (2014). The microbial metabolite butyrate regulates intestinal macrophage function via histone deacetylase inhibition. *Proc. Natl. Acad. Sci. USA* *111*, 2247–2252.
- Cummings, J.H. (1981). Short chain fatty acids in the human colon. *Gut* *22*, 763–779.
- Damjanovic, D., Small, C.L., Jeyanathan, M., McCormick, S., and Xing, Z. (2012). Immunopathology in influenza virus infection: uncoupling the friend from foe. *Clin. Immunol.* *144*, 57–69.
- De Filippo, C., Cavalieri, D., Di Paola, M., Ramazzotti, M., Poullet, J.B., Massart, S., Collini, S., Pieraccini, G., and Lionetti, P. (2010). Impact of diet in shaping gut microbiota revealed by a comparative study in children from Europe and rural Africa. *Proc. Natl. Acad. Sci. USA* *107*, 14691–14696.
- den Besten, G., van Eunen, K., Groen, A.K., Venema, K., Reijngoud, D.J., and Bakker, B.M. (2013). The role of short-chain fatty acids in the interplay between diet, gut microbiota, and host energy metabolism. *J. Lipid Res.* *54*, 2325–2340.
- DeSantis, T.Z., Hugenholtz, P., Larsen, N., Rojas, M., Brodie, E.L., Keller, K., Huber, T., Dalevi, D., Hu, P., and Andersen, G.L. (2006). Greengenes, a chimera-checked 16S rRNA gene database and workbench compatible with ARB. *Appl. Environ. Microbiol.* *72*, 5069–5072.
- Dienz, O., Rud, J.G., Eaton, S.M., Lanthier, P.A., Burg, E., Drew, A., Bunn, J., Suratt, B.T., Haynes, L., and Rincon, M. (2012). Essential role of IL-6 in protection against H1N1 influenza virus by promoting neutrophil survival in the lung. *Mucosal Immunol.* *5*, 258–266.
- Donohoe, D.R., Garge, N., Zhang, X., Sun, W., O'Connell, T.M., Bunger, M.K., and Bultman, S.J. (2011). The microbiome and butyrate regulate energy metabolism and autophagy in the mammalian colon. *Cell Metab.* *13*, 517–526.
- Edgar, R.C. (2010). Search and clustering orders of magnitude faster than BLAST. *Bioinformatics* *26*, 2460–2461.
- Fogg, D.K., Sibon, C., Miled, C., Jung, S., Aucouturier, P., Littman, D.R., Cumanan, A., and Geissmann, F. (2006). A clonogenic bone marrow progenitor specific for macrophages and dendritic cells. *Science* *311*, 83–87.
- Geissmann, F., Manz, M.G., Jung, S., Sieweke, M.H., Merad, M., and Ley, K. (2010). Development of monocytes, macrophages, and dendritic cells. *Science* *327*, 656–661.

- Holscher, H.D., Caporaso, J.G., Hooda, S., Brulc, J.M., Fahey, G.C., Jr., and Swanson, K.S. (2015). Fiber supplementation influences phylogenetic structure and functional capacity of the human intestinal microbiome: follow-up of a randomized controlled trial. *Am. J. Clin. Nutr.* *101*, 55–64.
- Hu, G.X., Chen, G.R., Xu, H., Ge, R.S., and Lin, J. (2010). Activation of the AMP activated protein kinase by short-chain fatty acids is the main mechanism underlying the beneficial effect of a high fiber diet on the metabolic syndrome. *Med. Hypotheses* *74*, 123–126.
- Jacobs, S.R., Herman, C.E., Maciver, N.J., Wofford, J.A., Wieman, H.L., Hammen, J.J., and Rathmell, J.C. (2008). Glucose uptake is limiting in T cell activation and requires CD28-mediated Akt-dependent and independent pathways. *J. Immunol.* *180*, 4476–4486.
- Kim, C.H., Park, J., and Kim, M. (2014). Gut microbiota-derived short-chain Fatty acids, T cells, and inflammation. *Immune Netw.* *14*, 277–288.
- Kim, M., Qie, Y., Park, J., and Kim, C.H. (2016). Gut microbial metabolites fuel host antibody responses. *Cell Host Microbe* *20*, 202–214.
- Kruger, P., Saffarzadeh, M., Weber, A.N., Rieber, N., Radsak, M., von Bernuth, H., Benarafa, C., Roos, D., Skokowa, J., and Hartl, D. (2015). Neutrophils: Between host defence, immune modulation, and tissue injury. *PLoS Pathog.* *11*, e1004651.
- Labonte, A.C., Tosello-Tramont, A.C., and Hahn, Y.S. (2014). The role of macrophage polarization in infectious and inflammatory diseases. *Mol. Cells* *37*, 275–285.
- Landsman, L., and Jung, S. (2007). Lung macrophages serve as obligatory intermediate between blood monocytes and alveolar macrophages. *J. Immunol.* *179*, 3488–3494.
- Landsman, L., Varol, C., and Jung, S. (2007). Distinct differentiation potential of blood monocyte subsets in the lung. *J. Immunol.* *178*, 2000–2007.
- Le Poul, E., Loison, C., Struyf, S., Springael, J.Y., Lannoy, V., Decobecq, M.E., Brezillon, S., Dupriez, V., Vassart, G., Van Damme, J., et al. (2003). Functional characterization of human receptors for short chain fatty acids and their role in polymorphonuclear cell activation. *J. Biol. Chem.* *278*, 25481–25489.
- Marko, A.J., Miller, R.A., Kelman, A., and Frauwirth, K.A. (2010). Induction of glucose metabolism in stimulated T lymphocytes is regulated by mitogen-activated protein kinase signaling. *PLoS ONE* *5*, e15425.
- Martínez, I., Kim, J., Duffy, P.R., Schlegel, V.L., and Walter, J. (2010). Resistant starches types 2 and 4 have differential effects on the composition of the fecal microbiota in human subjects. *PLoS ONE* *5*, e15046.
- Maslowski, K.M., Vieira, A.T., Ng, A., Kranich, J., Sierro, F., Yu, D., Schilter, H.C., Rolph, M.S., Mackay, F., Artis, D., et al. (2009). Regulation of inflammatory responses by gut microbiota and chemoattractant receptor GPR43. *Nature* *461*, 1282–1286.
- Millard, A.L., Mertes, P.M., Ittelet, D., Villard, F., Jeannesson, P., and Bernard, J. (2002). Butyrate affects differentiation, maturation and function of human monocyte-derived dendritic cells and macrophages. *Clin. Exp. Immunol.* *130*, 245–255.
- Nahrendorf, M., Swirski, F.K., Aikawa, E., Stangenberg, L., Wurdinger, T., Figueiredo, J.L., Libby, P., Weissleder, R., and Pittet, M.J. (2007). The healing myocardium sequentially mobilizes two monocyte subsets with divergent and complementary functions. *J. Exp. Med.* *204*, 3037–3047.
- Nsiah-Sefaa, A., and McKenzie, M. (2016). Combined defects in oxidative phosphorylation and fatty acid  $\beta$ -oxidation in mitochondrial disease. *Biosci. Rep.* *36*, 36.
- O’Sullivan, D., and Pearce, E.L. (2015). Targeting T cell metabolism for therapy. *Trends Immunol.* *36*, 71–80.
- Osthus, R.C., Shim, H., Kim, S., Li, Q., Reddy, R., Mukherjee, M., Xu, Y., Wonsey, D., Lee, L.A., and Dang, C.V. (2000). Deregulation of glucose transporter 1 and glycolytic gene expression by c-Myc. *J. Biol. Chem.* *275*, 21797–21800.
- Palmer, C.S., Ostrowski, M., Balderson, B., Christian, N., and Crowe, S.M. (2015). Glucose metabolism regulates T cell activation, differentiation, and functions. *Front. Immunol.* *6*, 1.
- Park, J., Kim, M., Kang, S.G., Jannasch, A.H., Cooper, B., Patterson, J., and Kim, C.H. (2015). Short-chain fatty acids induce both effector and regulatory T cells by suppression of histone deacetylases and regulation of the mTOR-S6K pathway. *Mucosal Immunol.* *8*, 80–93.
- Perrone, L.A., Plowden, J.K., García-Sastre, A., Katz, J.M., and Tumpey, T.M. (2008). H5N1 and 1918 pandemic influenza virus infection results in early and excessive infiltration of macrophages and neutrophils in the lungs of mice. *PLoS Pathog.* *4*, e1000115.
- Roy, M., Richard, J.F., Dumas, A., and Vallières, L. (2012). CXCL1 can be regulated by IL-6 and promotes granulocyte adhesion to brain capillaries during bacterial toxin exposure and encephalomyelitis. *J. Neuroinflammation* *9*, 18.
- Shirey, K.A., Pletneva, L.M., Puche, A.C., Keegan, A.D., Prince, G.A., Blanco, J.C., and Vogel, S.N. (2010). Control of RSV-induced lung injury by alternatively activated macrophages is IL-4R alpha-, TLR4-, and IFN-beta-dependent. *Mucosal Immunol.* *3*, 291–300.
- Smith, P.M., Howitt, M.R., Panikov, N., Michaud, M., Gallini, C.A., Bohlooly-Y, M., Glickman, J.N., and Garrett, W.S. (2013). The microbial metabolites, short-chain fatty acids, regulate colonic Treg cell homeostasis. *Science* *341*, 569–573.
- Trompette, A., Gollwitzer, E.S., Yadava, K., Sichelstiel, A.K., Sprenger, N., Ngom-Bru, C., Blanchard, C., Junt, T., Nicod, L.P., Harris, N.L., and Marsland, B.J. (2014). Gut microbiota metabolism of dietary fiber influences allergic airway disease and hematopoiesis. *Nat. Med.* *20*, 159–166.
- van der Windt, G.J., Everts, B., Chang, C.H., Curtis, J.D., Freitas, T.C., Amiel, E., Pearce, E.J., and Pearce, E.L. (2012). Mitochondrial respiratory capacity is a critical regulator of CD8+ T cell memory development. *Immunity* *36*, 68–78.
- Vinolo, M.A., Hatanaka, E., Lambertucci, R.H., Newsholme, P., and Curi, R. (2009). Effects of short chain fatty acids on effector mechanisms of neutrophils. *Cell Biochem. Funct.* *27*, 48–55.
- Wang, N., Liang, H., and Zen, K. (2014). Molecular mechanisms that influence the macrophage m1-m2 polarization balance. *Front. Immunol.* *5*, 614.
- Wieman, H.L., Wofford, J.A., and Rathmell, J.C. (2007). Cytokine stimulation promotes glucose uptake via phosphatidylinositol-3 kinase/Akt regulation of Glut1 activity and trafficking. *Mol. Biol. Cell* *18*, 1437–1446.
- WorldHealthOrganization (2016). Influenza (Seasonal). <http://www.who.int/mediacentre/factsheets/fs211/en/>.

## STAR★METHODS

## KEY RESOURCES TABLE

REAGENT or RESOURCE	SOURCE	IDENTIFIER
Antibodies		
InVivoMAb rat anti-mouse Ly6G, clone 1A8	BioXCell	Cat# BE0075-1; RRID: AB_1107721
InVivoMAb rat IgG2a isotype control, clone 2A3	BioXCell	Cat# BE0089; RRID: AB_1107769
Anti-mouse CD11c, APC/Cy7, clone N418	Biolegend	Cat#117323; RRID: AB_830646
Anti-mouse CD11b, Pacific Blue, clone M1/70	Biolegend	Cat# 101223; RRID: AB_755985
Anti-mouse Gr-1, PE/Cy5, clone RB6-8C5	Thermo Fisher Scientific	Cat# 15-5931-82; RRID: AB_468813
Anti-mouse CD11b, PerCP-Cy5.5, clone M1/70	Biolegend	Cat# 101228; RRID: AB_893232
Anti-mouse F4/80, Alexa Fluor 647, clone BM8	Biolegend	Cat# 123122; RRID: AB_893480
Anti-mouse I-A/I-E, Alexa Fluor 700, clone M5/114.15.2	Biolegend	Cat# 107622; RRID: AB_493727
Anti-mouse Ly6-c, Pacific Blue, clone HK1.4	Biolegend	Cat# 128014; RRID: AB_1732079
Anti-mouse CCR2, PE/Cy7, clone SA203G11	Biolegend	Cat# 150611; RRID: AB_2616983
Anti-mouse CX3CR1, PE, clone SA011F11	Biolegend	Cat# 149005; RRID: AB_2564314
Anti-mouse CD40, PE, clone 3/23	Biolegend	Cat# 124610; RRID: AB_1134075
Anti-mouse CD70, PE, clone FR70	Biolegend	Cat# 104605; RRID: AB_313118
Anti-mouse CD206, PE, clone C068C2	Biolegend	Cat# 141705; RRID: AB_10896421
Anti-mouse PD-L2, PE, clone TY25	Biolegend	Cat# 107205; RRID: AB_2299418
Anti-mouse CD86, biotin, clone GL-1	Biolegend	Cat# 105003; RRID: AB_313146
Streptavidin, PE/Cy7	Biolegend	Cat# 405206
Rabbit anti-mouse CXCL1, unlabeled, clone 1174A	R&D Systems	Cat# MAB4532
Goat anti-rabbit IgG, PE	R&D Systems	Cat# F0110; RRID: AB_573126
Anti-mouse CD45.2, Alexa Fluor 700, clone 104	Biolegend	Cat# 109822; RRID: AB_493731
Anti-mouse CD3, Pacific Blue, clone 17A2	Biolegend	Cat# 100214; RRID: AB_493645
Anti-mouse CD4, APC, clone GK1.5	Biolegend	Cat# 100412; RRID: AB_312697
Anti-mouse CD4, PerCP-Cy5.5, clone GK1.5	Biolegend	Cat# 100434; RRID: AB_893324
Anti-mouse CD8 $\alpha$ , PE/Cy7, clone 53-6.7	Biolegend	Cat# 100722; RRID: AB_312761
Anti-mouse CD62-L, PerCP-Cy5.5, clone MEL-14	Biolegend	Cat# 104432; RRID: AB_2285839
Anti-mouse CD107 $\alpha$ , APC/Cy7, clone 1D4B	Biolegend	Cat# 121615; RRID: AB_10640451
Anti-mouse Granzyme B, FITC, clone GB11	Biolegend	Cat# 515403; RRID: AB_2114575
Anti-mouse IFN $\gamma$ , APC, clone XMG1.2	Biolegend	Cat# 505810; RRID: AB_315404
Anti-mouse TNF $\alpha$ , Alexa Fluor 488, clone MP6-XT22	Biolegend	Cat# 506313; RRID: AB_493328
MHCI Multimer against Influenza NP-peptide (TYQRTRALV), PE	TCF UNIL	Cat# 220036
Anti-mouse Glut-1, PE	Novus Biologicals	Cat# NB110-39113PE
Anti-mouse Glut-1, Alexa Fluor 488	Novus Biologicals	Cat# NB110-39113AF488
Anti-mouse c-myc, Alexa Fluor 647, clone 9E10	Novus Biologicals	Cat# NB600-302AF647
Anti-mouse Ly6-A/E, PE/Cy7, clone D7	Biolegend	Cat# 108113; RRID: AB_493597
Anti-mouse CD117, Alexa Fluor 647, clone 2B8	Biolegend	Cat# 105817; RRID: AB_493475
Anti-mouse CD16/32, APC/Cy7, clone 93	Biolegend	Cat# 101327; RRID: AB_1967102
Anti-mouse CD34, PerCP-Cy5.5, clone HM34	Biolegend	Cat# 128607; RRID: AB_1279222
Anti-mouse CD135, PE, clone A2F10	Biolegend	Cat# 135305; RRID: AB_1877218
Anti-mouse CD11c, FITC, clone N418	Thermo Fisher Scientific	Cat# 11-0114-81; RRID: AB_464939
Anti-mouse Lineage Cocktail	Biolegend	Cat# 133310; RRID: AB_11150779
InVivoMAb rat anti-mouse CD3 $\epsilon$ , clone 145-2C11	BioXCell	Cat# BE0001-1; RRID: AB_1107634
InVivoMAb rat anti-mouse CD28, clone 37.51	BioXCell	Cat# BE0015-1; RRID: AB_1107624

(Continued on next page)

**Continued**

REAGENT or RESOURCE	SOURCE	IDENTIFIER
<b>Bacterial and Virus Strains</b>		
Influenza strain PR8 (A/Puerto Rico/8/34, H1N1)	Virapur LLC	N/A (custom production)
<b>Chemicals, Peptides, and Recombinant Proteins</b>		
Sodium Butyrate	Sigma-Aldrich	Cat# 303410-100G
Recombinant mouse M-CSF	Peptotech	Cat# 315-02-10UG
Recombinant mouse IFN $\gamma$	Peptotech	Cat# 315-05-100UG
Recombinant mouse IL-4	Peptotech	Cat# 214-14
Tri Reagent	MRC	TR118
Diff-Quik Solution	Dade Behring	Cat# 130832
Sodium Pentobarbital "Esconarkon"	Streuli Pharma	Cat# V102013
Acetyl methylcholine	Sigma	Cat# A2251-25G
Recombinant mouse CXCL1	Peptotech	Cat# 11-250
Influenza NP-peptide (H2-K <sup>d</sup> ; TYQRTRALV), unlabeled	TCF UNIL	Cat# 220036
Carboxyfluorescein succinimidyl ester (CFSE)	Enzo Life Sciences	Cat# ALX-610-030-M025
Collagenase IV	Thermo Fisher Scientific	Cat# 17104-019
Brefeldin A	Biologend	Cat# 420601
Saponin	Sigma-Aldrich	Cat# 47036-50G-F
MitoTracker Green FM dye	Life Technologies	Cat# M-7514
Nuclease-free Water	QIAGEN	Cat# 129115
AccuPrime Taq DNA Polymerase High Fidelity Assay	Thermo Fisher Scientific	Cat# 12346-086
Agencourt AMPure XP magnetic beads	Beckman Coulter	Cat# A63880
Sso Advanced SYBR Green Mix	Bio-Rad	Cat# 172-5274
2-(N-(7-Nitrobenz-2-oxa-1,3-diazol-4-yl)Amino)-2-Deoxyglucose	Sigma-Aldrich	Cat# 72987
Etomoxir Sodium Salt	Sigma-Aldrich	Cat# E1905
Cell-Tak Cell and Tissue Adhesive	Corning	Cat# 354240
Antimycin A	Sigma-Aldrich	Cat# A8674
Sodium Oleate	Sigma-Aldrich	Cat# O7501
Carnitine	Sigma-Aldrich	Cat# C0283
Rotenone	Sigma-Aldrich	Cat# R8875
Oligomycin	Sigma-Aldrich	Cat# O4876
FCCP	Sigma-Aldrich	Cat# C2920
<b>Critical Commercial Assays</b>		
Myeloperoxidase ELISA kit	Hycult Biotech	Cat# HK210
Mouse Albumin ELISA kit	ICL	Cat# E-90AL
IL-6, IL-1 $\beta$ , CXCL1, CXCL2, and CCL3 ProcartaPlex assay	ThermoFisher Scientific	Cat# PPX-10-MXPRJ2E
QiaAMP Fast DNA Stool Mini Kit	QIAGEN	Cat# 51604
Mouse CD8 T cell Isolation Kit	Miltenyi Biotec	Cat# 130-104-075
Mouse T cell activation / expansion kit	Miltenyi Biotec	Cat# 130-093-627
<b>Experimental Models: Organisms/Strains</b>		
Mouse: Ffar3 <sup>-/-</sup>	From NIBR, Basel, Switzerland	N/A
Mouse: Ffar2 <sup>-/-</sup>	From NIBR, Basel, Switzerland	N/A
Mouse: Cd8 <sup>-/-</sup> ; B6.129S2-cd8a <sup>tm1Mak/J</sup>	From LASC, Zurich, Switzerland	N/A
Mouse: Ly5.1: B6.SJL-Ptprc <sup>a</sup> Pepc <sup>b</sup> /BoyCrI	Charles River Laboratories	N/A
Mouse: C57BL/6: C57BL/6J	Charles River Laboratories	JAX Cat# 000664
Mouse: BALB/c: BALB/cByJ	Charles River Laboratories	JAX Cat# 001026

(Continued on next page)

**Continued**

REAGENT or RESOURCE	SOURCE	IDENTIFIER
Oligonucleotides		
Modified 27F universal primer targeting the V1-V2 hypervariable region of the 16S rRNA gene: 27F-5'- <b>AATGATACGGCGACCACCGAGATCTACAC</b> TATGGTAAT TCCAGMGTTYGATYMTGGCTCAG-3'	This paper	N/A
Modified 338R universal primers targeting the V1-V2 hypervariable region of the 16S rRNA gene: 338R-5'- <b>CAAGCAGAAGACGGCATACGAGAT</b> NNNNNNN NNN NNNAGTCAGTCAGAAGCTGCCTCCCGTAGGAGT-3'	This paper	N/A
Primers for quantitative PCR, see Table S1	This paper	N/A
Software and Algorithms		
GraphPad Prism 7.0c	GraphPad Software	<a href="https://www.graphpad.com/scientific-software/prism/">https://www.graphpad.com/scientific-software/prism/</a>
Dionex Chromeleon version 6.8	Thermo Fisher Scientific	<a href="https://www.thermofisher.com/order/catalog/product/CHROMELEON6">https://www.thermofisher.com/order/catalog/product/CHROMELEON6</a>
FlowJo LLC version 10.4.2	Becton Dickinson	<a href="https://www.flowjo.com/solutions/flowjo/downloads">https://www.flowjo.com/solutions/flowjo/downloads</a>
QIIME version 1.9.0	Caporaso et al., 2010	N/A
Uclust	Edgar, 2010	N/A
R	GNU Project	<a href="https://www.r-project.org/">https://www.r-project.org/</a>
CFX Manager™ version 2.1	Bio-Rad	N/A
Other		
Low Fiber Diet	KLIBA NAFAG	Cat# 2122
Cellulose "VITACEL"	J. Rettenmaier (JRS)	Cat# LC200
Inulin, "Fibrulin Instant"	Cosucra	Cat# 110472450
2 ml Biopure tubes	Eppendorf	Cat# 0030.121.597

**CONTACT FOR REAGENT AND RESOURCE SHARING**

Further information and requests for resources and reagents should be directed to and will be fulfilled by the Lead Contact, B. J. Marsland ([benjamin.marsland@monash.edu](mailto:benjamin.marsland@monash.edu)).

**EXPERIMENTAL MODEL AND SUBJECT DETAILS****Experimental Animals**

4-week-old BALB/c or C57BL/6 mice were purchased from Charles River Laboratories (L'Arbresle, France) and housed under specific pathogen-free conditions. *Ffar3*<sup>-/-</sup> and *Ffar2*<sup>-/-</sup> mice (both on a C57BL/6 background) were originally obtained from Novartis Institutes for Biomedical Research, Basel, Switzerland. Mice were fed specific diets for 4 to 6 weeks before being used for breeding or short-chain fatty acid (SCFA) supplementation experiments. *Cd8*<sup>-/-</sup> mice were originally obtained from the Laboratory Animal Services Center (LASC), Zurich, Switzerland. *Ly5.1* C57BL/6 mice were purchased from Charles River Laboratories. We used 8-12 week-old female mice for all experiments. All animal experiments were performed in accordance with institutional guidelines and Swiss federal and cantonal laws on animal protection.

**Rodent Diets**

Mice were fed a low-fiber diet (KLIBA NAFAG diet 2122) either supplemented with 30% inulin (fibrulin instant, Cosucra) or 30% cellulose (J. Rettenmaier & Söhne, Rosenberg, Germany). For SCFA-supplementation experiments, mice were fed a low-fiber diet (KLIBA NAFAG diet 2122) without any additives. All diets were purchased from Kliba Nafag AG, Kaiseraugst, Switzerland.

**SCFA Treatment**

Adult female mice were fed a low-fiber diet (KLIBA NAFAG diet 2122) for 4 weeks prior to and throughout the experiment. Mice then received sodium butyrate (Sigma-Aldrich, St. Louis, MO) in the drinking water at a final concentration of 500 mM for 2 weeks prior to influenza infection and throughout the whole study.

### Animal Model of Influenza A Infection

Adult (8–12 week-old) female mice were anaesthetized with a mixture of ketamine and xylazine (Dr. E. Graeb AG, Bern, Switzerland) and infected intranasally with varying doses of the influenza virus strain PR8 (A/Puerto Rico8/34, H1N1) (Virapur LLC, San Diego, CA) in 50  $\mu$ L sterile phosphate-buffered saline (PBS). Airway inflammation was examined at either day 1, 3, 5, 7 or 8 after infection. 1,100 PFU were used for high-dose infection of BALB/c, 4,500 PFU for high-dose infection in C57BL/6, and 100 PFU for low-dose infections. Mice were monitored daily during the course of infection and euthanized when reaching a weight loss of 15%–20% or a body temperature below 33°C.

### In Vitro Bone Marrow Differentiation Cultures

Tibia and femur from hind legs of 8–12 week-old female mice fed a control diet were extracted and bone marrow cells were flushed out into complete RPMI medium (GIBCO). Cell counts were determined using a Coulter Counter and  $1 \times 10^7$  cells were then plated in a 100  $\times$  20 mm cell culture Petri dish (Corning) containing 10 mL complete RPMI medium containing 10% L929 hybridoma supernatant (generated in-house) for 7 days at 37°C and 5% CO<sub>2</sub>. At day 2, 5 mL of fresh complete RPMI medium supplemented with 10% L929 hybridoma supernatant were added. At day 5, 5 mL were gently removed from the culture and another 5 mL of fresh complete RPMI medium containing 10% L929 hybridoma supernatant were added. During the whole culture period butyrate was mixed into the culture medium at a concentration of 0, 5, 50, and 100  $\mu$ M. At day 7, supernatants were taken off, cells were washed once with complete RPMI and then scraped off the plate. Cells were then further used for polarization experiments.

### Bone Marrow Macrophage Polarization

Macrophages that were differentiated from bone marrow cells for 7 days in the presence or absence of butyrate were collected and counted using a Coulter Counter. Cells were plated at a density of  $2 \times 10^5$  cells per well in a 24-well plate (Costar) in complete RPMI (GIBCO) in the presence of 100 ng ml<sup>-1</sup> recombinant mouse M-CSF (Peprotech) for 24 h at 37°C and 5% CO<sub>2</sub>. For M0 cultures no further cytokines were added. For M1 cultures 500 ng ml<sup>-1</sup> IFN $\gamma$  (Peprotech) was added throughout the culture period. For M2 cultures 10 ng ml<sup>-1</sup> IL-4 (Peprotech) was added throughout the culture period. After 24 h, supernatants were removed and cells were lysed in 250  $\mu$ L Tri Reagent (Molecular Research Center Inc.) and subjected to RNA extraction.

## METHOD DETAILS

### Cellular Infiltration of the Airways

Broncho-alveolar lavage fluid (BALF) was collected to assess the cellular compartment of the airway lumen. Total cell numbers in the BALF were determined using a Coulter Counter (IG Instrumenten-Gesellschaft AG, Basel, Switzerland). Differential cell counts were performed on cytopspins stained with Diff-Quik solution (Dade Behring, Siemens Healthcare Diagnostics, Deerfield, IL). Percentages of eosinophils, neutrophils, macrophages and lymphocytes were determined by counting 200 cells per sample.

### Measurement of Lung Function

Lung resistance was quantified using the whole body-restrained plethysmograph system flexiVent (SCIREQ). Mice were anesthetized by intramuscular injection of 100 mg per kg body weight ketamine and intraperitoneal injection of 50 mg per kg body weight pentobarbital (Esconarkon, Streuli Pharma). Eight minutes later, mice were tracheotomized and mechanically ventilated at a rate of 200 breaths per min and a tidal volume of 10 mL per kg body weight. Airway hyper-responsiveness was measured by administering increasing doses of acetyl methylcholine (12.5, 25, 50 and 100 mg/ml) (Sigma).

### Histology

Whole lung or right lobes were fixed in 10 mL of 10% buffered formalin at 4°C and embedded into paraffin. Prepared sections (4  $\mu$ m) were stained with Haematoxylin and Eosin (H&E) reagents using standardized protocols and analyzed with an Axioskop 2 plus microscope equipped with an Axio-Cam HRc (Carl Zeiss Microimaging GmbH, Jena, Germany).

### ELISAs

The activity of neutrophilic myeloperoxidase was quantified in BALF of infected mice (7 days post-infection) using a mouse MPO ELISA kit (Hycult biotech, Uden, Netherlands). Vascular leakage was determined by quantification of serum albumin in the BALF seven days after influenza infection using a mouse Albumin ELISA kit (ICL, Portland, OR). Assays were performed according to manufacturer's instructions and the colorimetric reaction was read at 450 nm on the Synergy H1 microplate reader (Biotek, Luzern, Switzerland). IL-6, IL-1 $\beta$ , CXCL1, CXCL2, and CCL3 protein levels were quantified in BALF using a ProcartaPlex Assay System (Thermo Fisher Scientific). Assays were performed according to manufacturer's instructions and read on the Luminex 200 Multiplexing Instrument (Bio-Rad).

### In vivo Neutrophil Reduction

In order to diminish neutrophils, 8–12 week-old female BALB/c mice were injected intraperitoneally with 20  $\mu$ g anti-Ly6G (clone 1A8, BioXCell) in 200  $\mu$ L PBS on day -1 and 1. Control mice received 20  $\mu$ g of corresponding isotype control antibody (clone 2A3,

BioXCell). On day 0, mice were infected with 600 PFU of influenza A (strain PR8). Mice were monitored daily during the course of infection and euthanized when reaching a weight loss of 15%–20% or a body temperature below 33°C.

### **In vivo Neutrophil Chemoattraction Assay**

In order to test the capacity of neutrophils from mice fed a fiber-rich diet to respond to the main neutrophil chemoattractant CXCL1, 5 µg of CXCL1 (Peprotech) were instilled intranasally to 8–12 week-old female BALB/c mice fed a control or inulin-rich diet. Six hours post-administration, the presence of neutrophils in the lungs and BALF was assessed and quantified by flow cytometry.

### **In Vivo Killing Assay**

Spleens from naive 8–12 week-old female BALB/c mice were extracted, cut in small pieces and passed through a 70 µm cell strainer to obtain a single cell suspension. Splenocytes were RBC lysed, counted and resuspended at a concentration of  $5 \times 10^6$  ml<sup>-1</sup>. The cell suspension was then divided into two equal fractions. One fraction was kept unpulsed, the other one was pulsed with 1 µL ml<sup>-1</sup> of a 200 µM stock of NP-peptide (H2-K<sup>d</sup>; TYQRTRALV) (TCF UNIL, Lausanne, Switzerland) for 1 h at 37°C in a water bath. Afterward, cells were recounted and resuspended at a concentration of  $5 \times 10^7$  ml<sup>-1</sup>. Unpulsed cells were labeled with 5 µM of Carboxyfluorescein succinimidyl ester (CFSE; Enzo Life Sciences), whereas the NP-pulsed cells were labeled with 0.5 µM CFSE for 10 min at 37°C, resulting in a CFSE<sup>high</sup> unpulsed fraction and a CFSE<sup>low</sup> NP-pulsed fraction. Both fractions were recounted and mixed at a 1:1 ratio. The mixture was then resuspended in PBS at a concentration of  $1 \times 10^8$  ml<sup>-1</sup> and 200 µL were injected intravenously to control and HFD-fed mice 7 days after influenza infection with 100 PFU PR8. 14 hours later, mice were sacrificed and the mediastinal lymph nodes were extracted. The ratio between the CFSE<sup>low</sup> and CFSE<sup>high</sup> fraction was determined by flow cytometry to assess killing efficiency.

### **Flow Cytometry**

Characterization and phenotyping of the various cell types in lung were performed by flow cytometry. Lung tissue was digested using collagenase IV (Thermo Fisher Scientific) in Iscove's modified Dulbecco's medium for 45 min at 37°C. Samples were then filtered through a 70 µm cell strainer, washed and resuspended in PBS supplemented with 0.2% bovine serum albumin (BSA). Total cell counts were determined using a Coulter Counter and cells were then stained for flow cytometry. Neutrophils were identified using antibodies to CD11c-allophycocyanin (APC)/Cy7 (117324, 1:600), CD11b-pacific blue (101223, 1:600), and Gr-1-phycoerythrin (PE)/Cy5 (15-5931, Thermo Fisher Scientific, 1:800). Activation and frequency of pulmonary conventional and inflammatory dendritic cells (DCs) and those of the monocyte and macrophage subsets were assessed using antibodies to CD11c-APC/Cy7 (117324, 1:600), CD11b-PerCP/Cy5.5 (101228, 1:600), F4/80-Alexa Fluor (AF) 647 (123122, 1:500), I-A/I-E-AF700 (107622, 1:1,000), Ly6c-pacific blue (128014, 1:600), CCR2-PE/Cy7 (150611, 1:400), CX3CR1-PE (149005, 1:400), Gr-1-PE/Cy5 (15-5931, Thermo Fisher Scientific, 1:800), CD40-PE (124610, 1:400), CD70-PE (104605, 1:400), CD206-PE (141705, 1:400), PD-L2-PE (107205, 1:400), CD86-biotin (105003, 1:400), and streptavidin-PE/Cy7 (405206, 1:1,000). CXCL1 intracellular expression was assessed after 4h incubation with Brefeldin A (Biolegend) using an unlabelled primary antibody against murine CXCL1 (R&D Systems, MAB4532, 1:100) and a goat-anti-rabbit-PE secondary antibody (R&D Systems, F0110, 1:50) to visualize the signal. To determine its expression in CD45<sup>neg</sup> cells, lungs were stained with CD45.2-AF700 (109822, 1:400). CD8<sup>+</sup> T cell numbers and activation were characterized by staining with antibodies to CD3-pacific blue (100214, 1:400), CD4-APC (100412, 1:600) or CD4-PerCP/Cy5.5 (100434, 1:600), CD8α-PE/Cy7 (100722, 1:800), CD62L-PerCP/Cy5.5 (104432, 1:600), and CD107α-APC/Cy7 (121615, 1:400), and intracellular staining using a 0.5% solution of saponin from Quillaja bark (Sigma-Aldrich) and antibodies to Granzyme B-FITC (515403, 1:100), IFNγ-APC (505810, 1:200), and TNFα-AF488 (506313, 1:200). Influenza A-specific CD8<sup>+</sup> T cells were identified using a MHC Multimer (PE-labeled) staining the nucleoprotein (NP) sequence TYQRTRALV (TCF UNIL, Lausanne, Switzerland). CD8<sup>+</sup> T cell metabolic state was determined using extra- or intracellular staining with an antibody to Glut-1-PE (NB110-39113PE, 1:400, Novus Biologicals) or -AF488 (NB110-39113AF488, 1:400, Novus Biologicals), and intracellular staining of *c-myc*-AF647 (NB600-302AF647, 1:400, Novus Biologicals). MitoTracker® Green FM dye (Life technologies) was used to mark mitochondria. For identification of progenitor cells, bone marrow was isolated from the left leg of mice. To distinguish different progenitor populations bone marrow cells were stained with antibodies to Ly-6A/E-PE/Cy7 (108113, 1:800), CD117-AF647 (105817, 1:400), CD16/32-APC/Cy7 (101327, 1:400), CD34-PerCP/Cy5.5 (128607, 1:300), CD135-PE (135305, 1:400), CD11c-FITC (11-0114-81, 1:400, Thermo Fisher Scientific), I-A/I-E-AF700 (107622, 1:1,000), and a Lineage Cocktail-pacific blue (133310, 1:50). If not indicated otherwise, antibodies were purchased from Biolegend (San Diego, CA). Fluorescence minus one (FMO) internal staining controls were set up by pooling cells from all the different experimental groups. Cells were acquired on BD Fortessa or LSR-II (BD Biosciences, San Jose, CA). Samples were analyzed using FlowJo 10.4.2 software (Tree Star Inc., Ashland, OR).

### **Metabolite screening**

Metabolite analysis by LC–tandem mass spectrometry was performed using a LCMS-8050 by Shimadzu triple quadrupole mass spectrometer equipped with an electrospray ionization (ESI) source and operated in multiple reaction mode (MRM). For graphical representation in a heatmap, the data is arranged in a matrix, in which each metabolite is depicted in one row, each group is depicted in one column, and mean metabolite abundances in a specific group are illustrated by color. Each metabolite's abundances are centered and scaled. First, centring is done by subtracting the total metabolite's mean. Second, scaling is done by dividing the centered metabolite by its standard deviation. The resulting values are in a similar range for all metabolites.

### SCFA Quantification

Organic acids - acetate, propionate and butyrate - present in the feces of 8-12 week-old female BALB/c mice fed our different diets were analyzed by gas chromatography (GC) on DB-FFAP column, from Agilent Technologies 6890 series GC System with a FID detection. Briefly, feces were first homogenized in a solution of ortho-phosphoric acid 0.1%, Mercury chloride 0.1%, and 2,2 Dimethyl-Butyrate as internal standard, corresponding to 4 times the weight of feces. Samples were then homogenized with 2 mm glass beads for 20 min with a multivortex. Preparations were centrifuged at 2,000 g for 15 min at 4°C. Supernatants were collected and weighed. Subsequently, 10 µL HCl 37% and 3 mL of chloroform were added and homogenized for 20 min. After centrifugation for 10 min at 1,800 g and 4°C, the upper layer was eliminated. After addition of 10 µL T-butyldimethylsilylimidazole, samples were heated at 60°C for 30 min then cooled down before being injected. Freeze-drying to determine humidity rate and humidity content was used for the calculation of SCFA per gram of dry material. Serum samples were analyzed using the HPLC Ultimate 3000 (Dionex, Sunnyvale, CA) equipped with an U3000 RS diode array detector (Dionex). Sera were diluted in a 1:6 ratio with 25% meta-phosphoric acid, incubated on ice for 30 min before being centrifugated at 12,000 g for 15 min at 4°C. Supernatants were then applied onto a Ultrafree MC filtering unit (Merck Millipore) and spun down at 12,000 g for 4 min at 4°C. Eluates were analyzed by HPLC. SCFAs were separated on a Hi-Plex H column (8 mm; 300 × 7.7 mm; Polymer Laboratories (Varian), Shropshire, UK) run isocratic with 5 mM sulfuric acid at a flow rate of 0.6 mL per min and a temperature of 55°C. Organic acids were detected at a wavelength of 210 nm and quantified using external standard curves from 0.5 to 100 mM of the respective authentic organic acids (Sigma-Aldrich). Dionex Chromeleon software version 6.8 (Thermo Fisher Scientific) was employed to pilot the HPLC and determine the concentrations of each individual organic acid.

### Bacterial DNA Isolation from Mouse Feces

Feces from 8-12 week-old female BALB/c mice housed under specific pathogen-free conditions were harvested under sterile conditions in a 2 mL Biopure tube (Eppendorf, Hamburg, Germany) and immediately snap-frozen in liquid nitrogen. Samples were stored at -80°C until processing for DNA isolation. Total bacterial DNA from 1-2 fecal pellets were isolated using the QiaAmp Fast DNA Stool Mini Kit (QIAGEN) according to manufacturer's instructions. DNA was eluted in 80 µL DNase/RNase-free water (QIAGEN) and its concentration was determined using a Nanodrop ND-1000 spectrophotometer (Thermo Fisher Scientific, Asheville, NC). DNA was stored at 4°C until being used for sequencing.

### 16S rRNA Library Preparation and Sequencing

16S rRNA gene amplicon library was generated using modified 27F and 338R universal primers targeting the V1-V2 hypervariable region of the 16S rRNA gene. Primers were designed as follows: 27F-5'-**AATGATACGGCGACCACCGAGATCTACAC**TATGGT AATTCCAGMGTTYGATYMTGGCTCAG-3' and 338R-5'-**CAAGCAGAAGACGGCATACGAGAT**NNNNNNN NNNNNNAGTCAGTCA GAAGCTGCCTCCCGTAGGAGT-3' where Illumina adaptor sequences are bold, linkers italicized and NNNNNNNNNNNNN sequences represents the sample-specific MID tag barcodes. Each PCR reaction was performed in duplicates in 20 µL total volume using the AccuPrime Taq DNA polymerase high fidelity kit (Invitrogen) with 4 µL of DNA template and 0.44 µL of each 27F and 338R primers at 10 µM. Amplification conditions consisted of 3 min of initial denaturation at 94°C, followed by 30 cycles of 30 s of denaturation at 94°C, 30 s of annealing at 56°C, and 90 s of extension with 5 min of final extension at 72°C. Amplicons size and quantity was assessed on the LabChip GX (Perkin Elmer) before combining PCR products in equimolar amounts of amplicons. Pooled library was purified using Agencourt AMPure XP magnetic beads (Beckman Coulter) and sequencing was performed on an Illumina MiSeq platform with MiSeq reagent kit V2-500 (pair-end, 2x250).

### 16S rRNA Gene Sequencing Data Analysis

16S rRNA sequences were processed and analyzed using Quantitative Insights Into Microbial Ecology (QIIME, v.1.9.0) software (Caporaso et al., 2010). Merging of paired forward and reverse reads was performed using fastq-join before demultiplexing and quality filtering (quality Phred score Q > 20, < 3 low quality base calls). Operational taxonomic units (OTUs) were assigned using a closed OTU picking strategy with Uclust (Edgar, 2010) at 97% identity against the 97% Greengenes reference database (v13.5) (DeSantis et al., 2006). Beta diversity was estimated using Bray-Curtis distance matrix generated in QIIME followed by principal component analysis using cmdscale in the R software. Statistical significance of differences in community composition was assessed by analysis of similarity (ANOSIM) with 100000 permutations using adonis command (vegan package) in the R software. Alpha diversity was assessed using chao1 and Shannon indexes calculated in QIIME. Unpaired Student's t tests were used to test for differences in alpha diversity between the two experimental groups. Significant differences in OTU abundance among experimental groups were assessed using Wilcoxon statistical procedure (runWilcox in EMA package) on filtered OTU table (> 0.001% of relative abundance) with P-value correction using Benjamini-Hochberg false discovery rate (FDR) with a corrected alpha value of 0.05. A heatmap was generated using heatmap.2 function (gplots package) in R with data representing row-scaled z-scores. Ward's hierarchical clustering (ward.D) and corresponding dendrogram were performed using hclust algorithm on Bray-Curtis dissimilarity matrix.

### Quantitative Polymerase Chain Reaction (qPCR)

Relative lung *Csf3*, *Il-4*, *Il-10*, *Ifn $\gamma$* , *Arg1*, *Nos2*, and *Cxcr2* mRNA expression as well as viral load was assessed by quantitative RT-PCR using the following primer sets: *Csf3* forward 5'-TGACACAGCTTGTAGGTGGC-3' and reverse 5'-TCCTGCTTAAGTCCCTG GAG-3'; *Il-4* forward 5'-TGTCATCTGCTCTTCTTCTC-3' and reverse 5'-GCACCTTGAAGCCCTAC-3'; *Il-10* forward

5'-GCATGGCCCCAGAAATCAAGG-3' and reverse 5'-AGAAATCGATGACAGCGCCTC-3'; *Ifn $\gamma$*  forward 5'-GCTCTGAGACAATGA ACGCTAC-3' and reverse 5'-TTCTAGGCTTTCAATGACTGTGCC-3'; influenza matrix protein (to determine viral load) forward 5'-CCCTGAAGTACCCATTGAAC-3' and reverse 5'-CTTTTCACGGTTGGCCTTAG-3'; *Arg1* forward 5'-GCAACCTGTGTCC TTTCTCC-3' and reverse 5'-TCTACGTCTCGCAAGCCAAT-3'; *Nos2* forward 5'-CTGCCTCATGCCATTGAGTT-3' and reverse 5'-TGAGCTGGTAGGTTCTCTGTTG-3'; *Cxcr2* forward 5'-ATCCACCTTGAATTCTCCCAT-3' and reverse 5'-GTCACAGAGAGTTGGG ACCC-3';  $\beta$ -*Actin* forward 5'-GATCAAGATCATTGCTCCTCC TGA-3' and reverse 5'-CAGCTCAGTAACAGTCCGCC-3'. Ten micro-liter PCR reactions were set up containing 2  $\mu$ L of template cDNA at a concentration of 50 ng ml<sup>-1</sup>, 5  $\mu$ L SsoAdvanced SYBR Green reaction mix (Bio-Rad, Hercules, CA), 0.25  $\mu$ L of each primer at a concentration of 20  $\mu$ M and 2.5  $\mu$ L of nuclease-free water. All reactions were performed in duplicates and each gene was normalized to  $\beta$ -actin. Quantitative PCR was performed on the CFX96 Touch Real-Time PCR Detection System (Bio-Rad) using the following conditions: one cycle at 95°C for 2 min and then 40 cycles at 95°C for 15 s and 60°C for 30 s, followed by a dissociation stage at 65°C for 31 s and cycles of 5 s starting at 65°C, raising 0.5°C per cycle, to obtain melting curves for specificity analysis. Following amplification, C<sub>q</sub> values were obtained using the CFX Manager™ software 2.1 (Bio-Rad).

### CD8<sup>+</sup> T Cell Adoptive Transfer

Splenic CD8<sup>+</sup> T cells from 8-12 week-old wild-type (*Ly5.1*) and *Ffar3*<sup>-/-</sup> (*Ly5.2*) female mice were obtained by negative selection using magnetic beads (Miltenyi Biotec), mixed in a 1:1 ratio and 6 × 10<sup>6</sup> CD8<sup>+</sup> T cells were transferred intravenously to *Cd8*<sup>-/-</sup> recipient mice, given water or butyrate orally. The purity of the selection, as well as the accuracy of the 1:1 ratio were determined by flow cytometry before being injected into the recipient mice. The day following the adoptive transfer, *Cd8*<sup>-/-</sup> mice were infected intranasally with influenza PR8. Mice were sacrificed eight days post-infection to evaluate the frequency and effector function of influenza-specific *Ly5.1*<sup>+</sup> and *Ly5.2*<sup>+</sup> CD8<sup>+</sup> T cells present in the lung by flow cytometry.

### Mixed Bone Marrow Chimeras

Bone marrow cells were obtained from 8-12 week-old wild-type (*Ly5.1*) and *Ffar3*<sup>-/-</sup> (*Ly5.2*) female mice, mixed in a 1:1 ratio and 5 × 10<sup>6</sup> cells were injected intravenously into lethally  $\gamma$ -irradiated 12 week-old C57BL/6 recipient mice (2 doses of 450 Rads spaced by a 4 hour interval between irradiations). Five weeks post-transfer, engraftment of donor cells was verified by flow cytometry by assessing the presence of *Ly5.1*<sup>+</sup> and *Ly5.2*<sup>+</sup> cells in the blood of recipient mice. Six weeks post-transfer, mice were infected intranasally with influenza PR8 and sacrificed three days post-infection. The proportions of *Ly5.1*<sup>+</sup> and *Ly5.2*<sup>+</sup>-derived Ly6c<sup>neg</sup> patrolling monocytes and interstitial macrophages present in the blood and lung of recipient mice were determined by flow cytometry.

### In Vitro CD8<sup>+</sup> T Cell Assays

CD8<sup>+</sup> T cells were isolated from the spleens of naive 8-12 week-old female mice fed a low-fiber diet either supplemented with 30% inulin or 30% cellulose by negative selection using magnetic beads (Miltenyi Biotec, Germany). Cells were plated in the presence of 5  $\mu$ g ml<sup>-1</sup> plate-coated anti-CD3 and 2  $\mu$ g ml<sup>-1</sup> soluble anti-CD28 and incubated for 1.5 h at 37°C and 5% CO<sub>2</sub>. Cells were then starved for an additional hour by removing glucose from the medium. At last, glucose-deprivation was reversed by re-adding medium containing 100  $\mu$ M 2-(N-(7-Nitrobenz-2-oxa-1,3-diazol-4-yl)Amino)-2-Deoxyglucose (2-DG) (Sigma-Aldrich) for 1 h prior to analysis. Metabolic state and activation of CD8<sup>+</sup> T cells from mice fed the different diets was compared by flow cytometry. To determine the direct effect of the SCFA butyrate on CD8<sup>+</sup> T cells, cells obtained from cellulose-fed mice were pooled and plated in the presence of 5  $\mu$ g ml<sup>-1</sup> plate-coated anti-CD3, 2  $\mu$ g ml<sup>-1</sup> soluble anti-CD28, and increasing doses of sodium butyrate (Sigma-Aldrich) for 24 h at 37°C and 5% CO<sub>2</sub>. 500  $\mu$ M etomoxir (Sigma-Aldrich) was added to the culture to block fatty acid oxidation. Metabolic state and activation of CD8<sup>+</sup> T cells in the presence or absence of sodium butyrate was compared using Flow cytometry.

### CD8<sup>+</sup> T Cell Metabolic Assays

CD8<sup>+</sup> T cells were isolated from the spleens of naive 8-12 week-old female mice fed a low-fiber diet either supplemented with 30% inulin or 30% cellulose by negative selection using magnetic beads (Miltenyi Biotec) and used for analysis of the metabolic phenotype. OCR (in pmoles/min) and ECAR (in mpH/min) were measured using the Seahorse XF-24 metabolic extracellular flux analyzer (Agilent) using two different experimental settings, a mitochondrial stress test and a glycolysis stress test. For the mitochondrial stress test, purified CD8<sup>+</sup> T cells were washed and resuspended in serum-free unbuffered KHB medium containing 25 mM Glucose, 2 mM Glutamine, 1 mM pyruvate, 150  $\mu$ M Oleate and 1.5 mM Carnitine. The cells were then plated onto Seahorse cell plates (7 × 10<sup>5</sup> cells per well) coated with Cell-Tak cell and tissue adhesive (Corning) to allow their attachment. Perturbation profiling of substrate use by CD8<sup>+</sup> T cells was achieved by addition of anti-CD3/CD28 beads (2 beads per cell) (Miltenyi Biotec, Germany), oligomycin (1  $\mu$ g ml<sup>-1</sup>), Carbonyl Cyanide 4-(trifluoromethoxy)phenylhydrazone (FCCP) (1.5  $\mu$ M) and rotenone (100 nM) plus Antimycin A (1  $\mu$ M). The maximal respiratory capacity was determined after addition of FCCP; the Spare Respiratory Capacity (SRC) was calculated as percent change between the basal respiration (in OCR) and the maximal respiratory capacity (in OCR). For the glycolysis stress test, purified CD8<sup>+</sup> T cells were washed and resuspended in serum-free unbuffered KHB medium containing only 2 mM Glutamine and 2 anti-CD3/28 beads per cell. The cells were then plated onto Seahorse cell plates (7 × 10<sup>5</sup> cells per well) coated with Cell-Tak to allow their attachment. Perturbation profiling of substrate use by CD8<sup>+</sup> T cells was achieved by addition of glucose (10 mM), oligomycin (1  $\mu$ g ml<sup>-1</sup>), and 2-DG (100 mM). The glutamine oxidation is the basal respiration (in OCR) since glutamine is the only substrate available for the cells. The glucose-dependent ECAR was calculated as the difference between the basal

extracellular acidification rate and the glucose-induced maximal glycolytic rate (in ECAR). Experiments with the Seahorse apparatus were done with the following assay conditions: 2 min mixture; 2 min wait; and 4-5 min measurements. All chemical compounds were purchased from Sigma-Aldrich.

### QUANTIFICATION AND STATISTICAL ANALYSIS

Student's t test (unpaired or paired, two-tailed), Mann-Whitney test (in the case of a non-Gaussian distribution of the samples) or Mantel-Cox test (for comparing groups in survival experiments) were used to calculate significance levels between treatment groups. Statistical tests used for microbiota analysis are indicated in the "16S rRNA Sequencing Data Analysis" of the "Method Details" section of the STAR methods. Statistical parameters are reported in each figure legend. n represents the number of biological replicates. All results are expressed as mean  $\pm$  SEM where SEM represents the Standard Error of the Mean. NS = not significant.  $p < 0.05$  was considered significant. \* $p < 0.05$ , \*\* $p \leq 0.01$ , \*\*\* $p \leq 0.001$ , \*\*\*\* $p \leq 0.0001$ . Variances were similar between compared groups in all experiments. No randomization strategy was used before conducting animal experiments. Investigators were not blinded when performing the experiments or analyses. Graph generation and statistical analyses were performed using Prism software version 7.0c (GraphPad, La Jolla, CA).

**Immunity, Volume 48**

**Supplemental Information**

**Dietary Fiber Confers Protection against Flu  
by Shaping Ly6c<sup>-</sup> Patrolling Monocyte Hematopoiesis  
and CD8<sup>+</sup> T Cell Metabolism**

**Aurélien Trompette, Eva S. Gollwitzer, Céline Pattaroni, Isabel C. Lopez-Mejia, Erika Riva, Julie Pernot, Niki Ubags, Lluís Fajas, Laurent P. Nicod, and Benjamin J. Marsland**

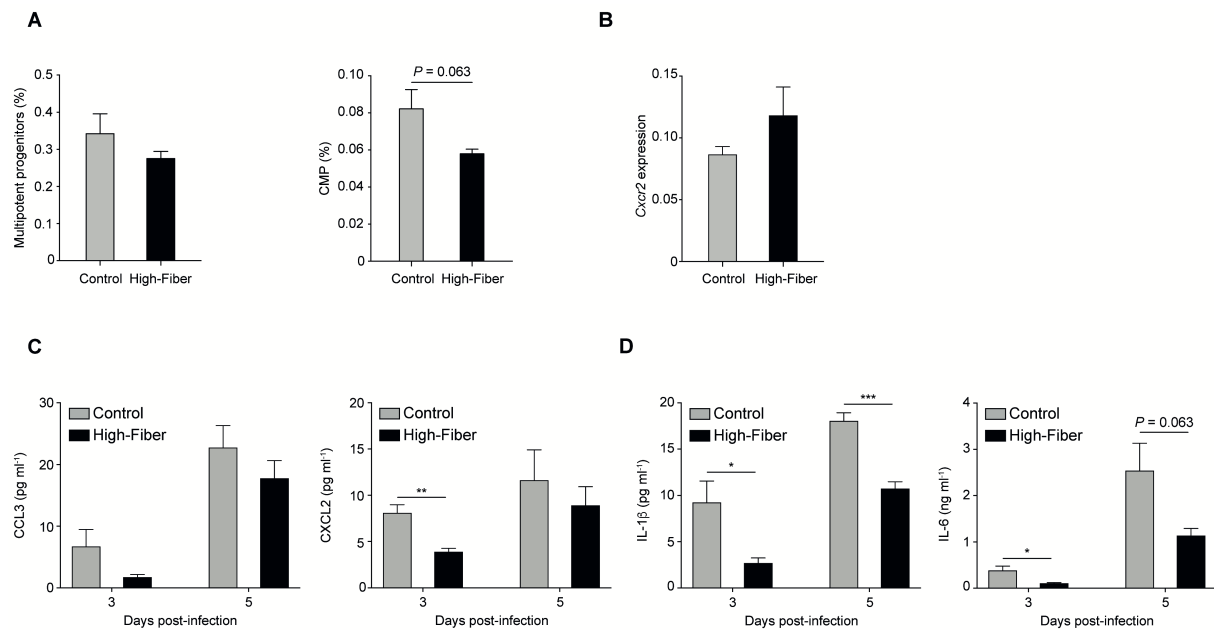


**Figure S1. Dietary fiber does not alter bone marrow granulopoiesis and neutrophil *Cxcr2* expression but does blunt the secretion of neutrophilia-promoting chemokines and cytokines in the lung. Related to Figure 3.** (A) Frequency of multipotent and common myeloid progenitor cells in the bone marrow of control or high fiber diet (HFD)-fed mice five days after low-dose infection. (B) Expression of the CXCL1 and CXCL2 receptor *Cxcr2* on purified neutrophils five days after low-dose infection. (C) Levels of the two neutrophil chemoattractants CCL3 and CXCL2 in the lung of control or HFD-fed mice three and five days after low-dose infection. (D) Levels of neutrophil-promoting cytokines IL-1 $\beta$  and IL-6 in the lung of control or HFD-fed mice three and five days after low-dose infection. Results are representative of data generated in two independent experiments and are expressed as mean  $\pm$  S.E.M. ( $n = 4$  control mice and  $n = 4$  mice on high-fiber diet). Results in A are representative of data generated in two independent experiments and are expressed as mean  $\pm$  S.E.M. ( $n = 4$  control mice and  $n = 4$  mice on high-fiber diet in C). Results in B are from two pooled independent experiments and are expressed as mean  $\pm$  S.E.M. ( $n = 3$  pooled from a total of eight control mice and  $n = 3$  pooled from a total of eight mice on high-fiber diet). Results in C and D are representative of data generated from four (day 3 post-infection time-point) or two to three (day 5 post-infection time-point) independent experiments and are expressed as mean  $\pm$  S.E.M. ( $n = 4$  control mice and  $n = 4$  mice on high-fiber diet). Statistical significance was determined with Student's *t*-test (unpaired, two-tailed). \* $P = 0.05$ , \*\* $P = 0.01$ , \*\*\* $P = 0.001$ .

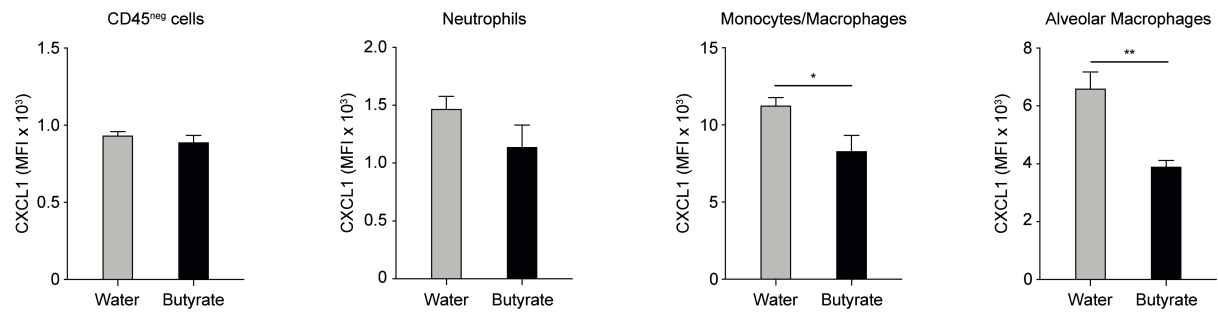


**Figure S2. The Short-Chain Fatty Acid Butyrate reduces the production of CXCL1 by macrophages in the lung. Related to Figure 3.** Intracellular expression of CXCL1 in CD45<sup>neg</sup> cells, neutrophils, F4/80<sup>+</sup> monocytes/macrophages and alveolar macrophages from lung of mice given butyrate orally five days after low-dose infection. MFI: Mean Fluorescence Intensity. Results are representative of data generated from two independent experiments and are expressed as mean  $\pm$  S.E.M. ( $n = 5$  control mice on water and  $n = 5$  mice on butyrate). Statistical significance was determined with Student's *t*-test (unpaired, two-tailed). \* $P = 0.05$ , \*\* $P = 0.01$ .

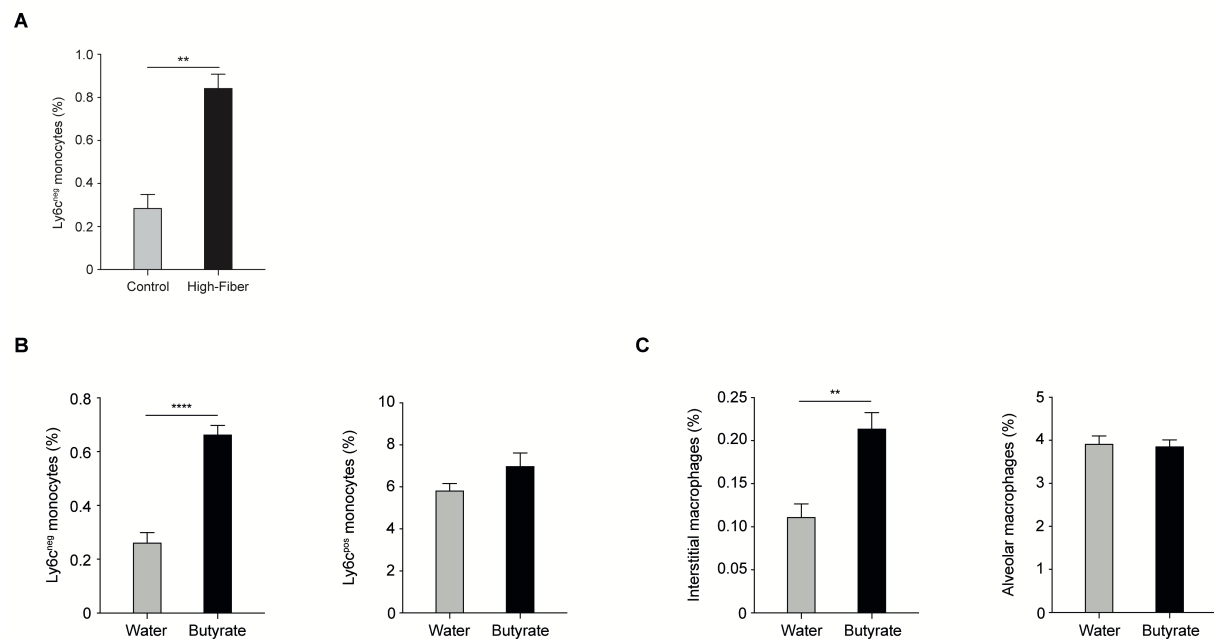


**Figure S3. Dietary fiber and the Short-Chain Fatty Acid butyrate promote the expansion of regulatory Ly6c<sup>neg</sup> patrolling monocytes and further-differentiated interstitial macrophages.**

**Related to Figure 4. (A)** Frequencies of Ly6c<sup>neg</sup> monocytes in the blood of mice fed a control or high-fiber diet three days after low-dose infection. **(B, C)** Frequencies of Ly6c<sup>neg</sup> and Ly6c<sup>pos</sup> monocytes **(B)** as well as interstitial and alveolar macrophages **(C)** in the lung of mice given butyrate orally five days after low-dose infection. Results are representative of data generated from two independent experiments and are expressed as mean  $\pm$  S.E.M. ( $n = 5$  control mice and  $n = 3$  mice on high-fiber diet;  $n = 5$  control mice on water and  $n = 5$  mice on butyrate). Statistical significance was determined with Student's *t*-test (unpaired, two-tailed). \*\* $P = 0.01$ , \*\*\*\* $P = 0.0001$ .

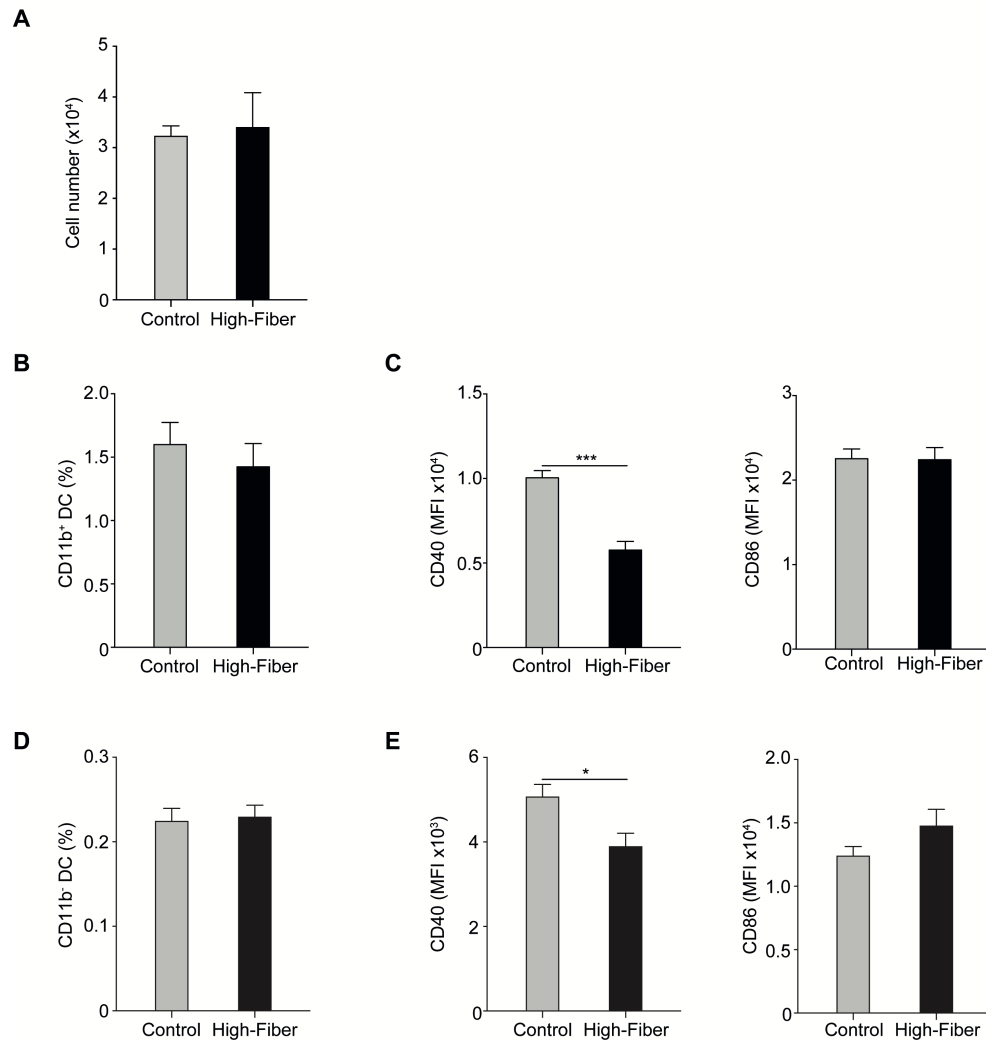


**Figure S4. Dietary fiber does not alter total lung lymphocytes and dendritic cells (DCs) early during infection. Related to Figure 5.** (A) Quantification of total lymphocyte numbers in the lung of control or HFD-fed mice five days after low-dose infection. (B) Frequency of CD11b<sup>+</sup> DCs in the lung of control or HFD-fed mice five days after low-dose infection. (C) Surface expression of CD40 and CD86 on CD11b<sup>+</sup> DCs in the lung of control or HFD-fed mice five days after low-dose infection. (D) Frequency of CD11b<sup>-</sup> DCs in the lung of control or HFD-fed mice five days after low-dose infection. (E) Surface expression of CD40 and CD86 on CD11b<sup>-</sup> DCs in the lung of control or HFD-fed mice five days after low-dose infection. MFI: Mean Fluorescence Intensity. Results are representative of data generated in two independent experiments and are expressed as mean  $\pm$  S.E.M. ( $n = 6$  control mice and  $n = 5$  mice on high-fiber diet). Statistical significance was determined with Student's *t*-test (unpaired, two-tailed). \* $P = 0.05$ , \*\*\* $P = 0.001$ .

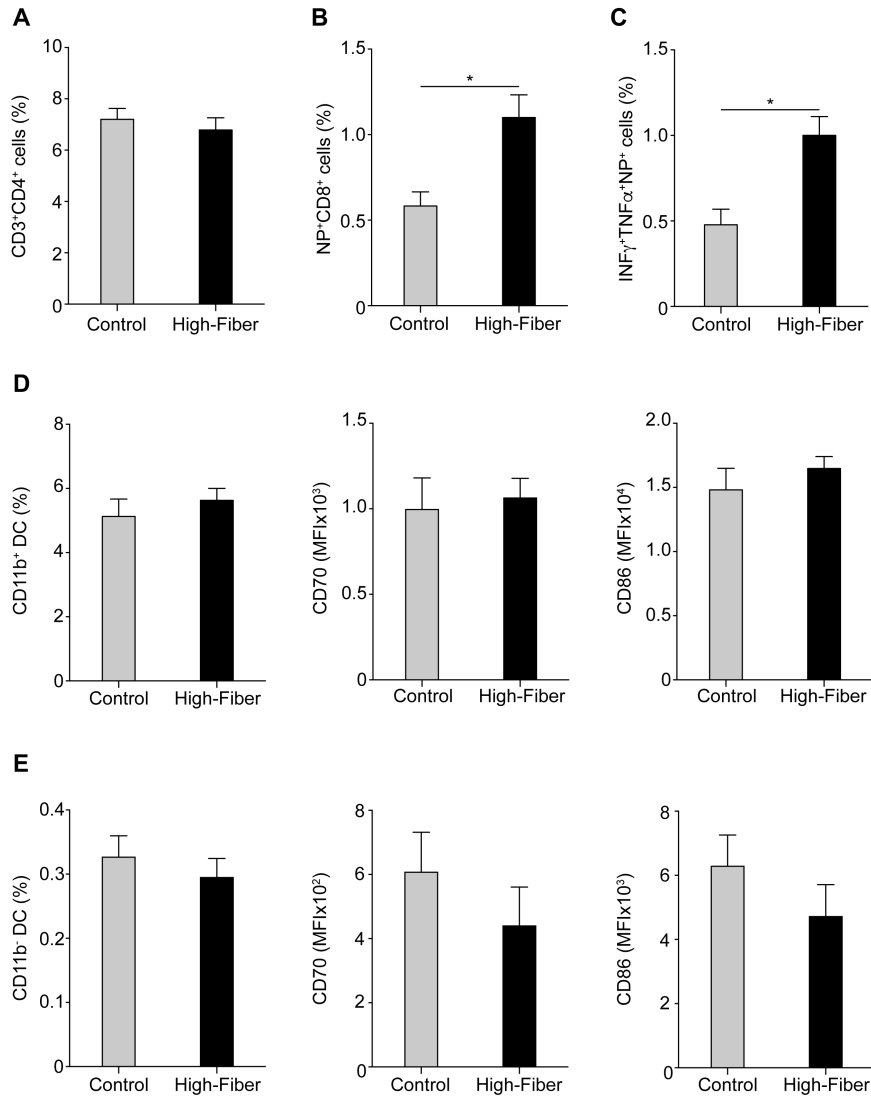


**Figure S5. Dietary fiber alters CD8<sup>+</sup> T cell responses without influencing dendritic cell (DC) activation later during infection. Related to Figure 5. (A)** Frequency of CD4<sup>+</sup> T cells in the lung of control or HFD-fed mice eight days after low-dose infection. **(B)** Frequency of influenza NP-positive CD8<sup>+</sup> T cells in the BALF of control or HFD-fed mice eight days after low-dose infection. **(C)** Frequency of IFN $\gamma$  and TNF $\alpha$  double-producing NP<sup>+</sup>CD8<sup>+</sup> T cells in the BALF of control or HFD-fed mice eight days after low-dose infection. **(D)** Frequency of CD11b<sup>+</sup> DCs in the lung and their surface expression of CD70 and CD86 ten days after low-dose infection. **(E)** Frequency of CD11b<sup>-</sup> DCs in the lung and their surface expression of CD70 and CD86 ten days after low-dose infection. MFI: Mean Fluorescence Intensity. Results are representative of data generated in two independent experiments and are expressed as mean  $\pm$  S.E.M. ( $n = 4$  control mice and  $n = 5$  mice on high-fiber diet). Statistical significance was determined with Student's *t*-test (unpaired, two-tailed). \* $P = 0.05$ .

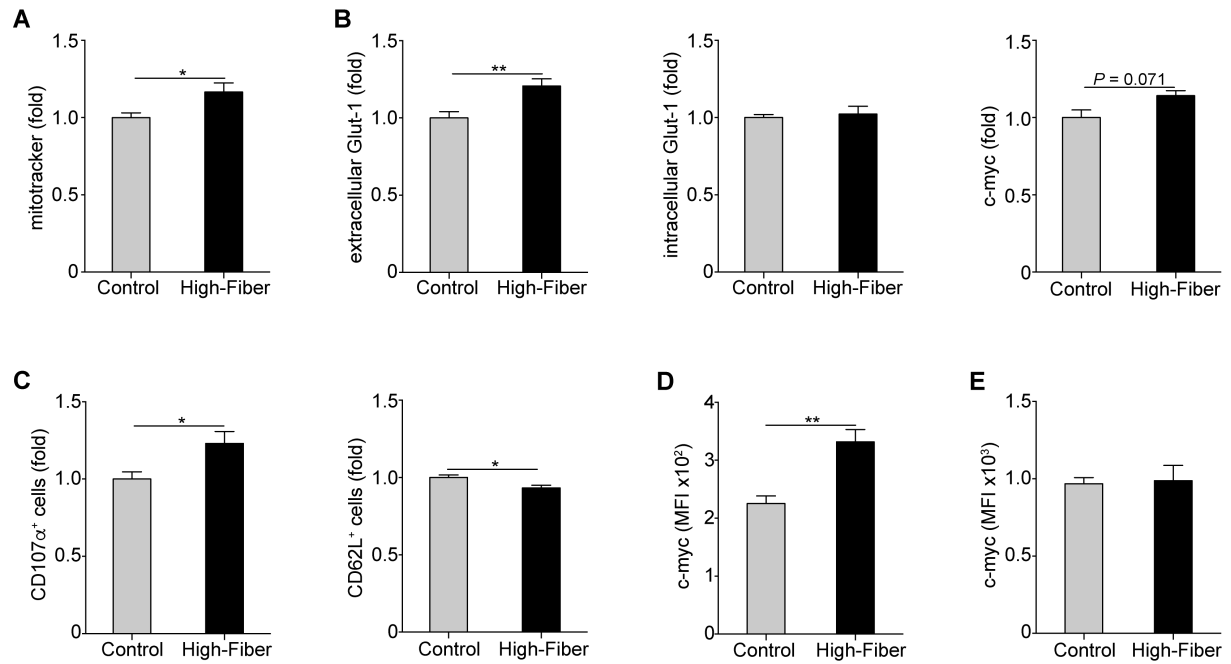


**Figure S6. Dietary fiber alters CD8<sup>+</sup> T cell metabolism. Related to Figure 6.** (A) Fold-change in mitochondrial mass as measured by mitotracker staining after a 4h *in vitro* activation and glucose-deprivation of naïve CD8<sup>+</sup> T cells isolated from control or HFD-fed mice. (B) Fold-change in surface and intracellular Glut-1 as well as c-myc expression after a 4h *in vitro* activation and glucose-deprivation of naïve CD8<sup>+</sup> T cells isolated from control or HFD-fed mice. (C) Fold-change in the frequency of CD107α and CD62L-expressing cells after a 4h *in vitro* activation and glucose-deprivation of naïve CD8<sup>+</sup> T cells isolated from control or HFD-fed mice. (D) Intracellular c-myc expression in pulmonary CD8<sup>+</sup> T cells from control or HFD-fed mice five days after low-dose infection. MFI: Mean Fluorescence Intensity. (E) Intracellular c-myc expression in pulmonary CD8<sup>+</sup> T cells from control or HFD-fed mice eight days after low-dose infection. MFI: Mean Fluorescence Intensity. Results are representative of data generated in two to three independent experiments and are expressed as mean ± S.E.M. ( $n = 6$  control mice and  $n = 6$  mice on high-fiber diet in **A-C**;  $n = 5$  control mice and  $n = 4$  mice on high-fiber diet in **D**;  $n = 4$  control mice and  $n = 5$  mice on high-fiber diet in **E**). Statistical significance was determined with Student's *t*-test (unpaired, two-tailed). \* $P = 0.05$ , \*\* $P = 0.01$ .

Gene	Forward	Reverse	Source
<i>Csf3</i>	TGACACAGCTTGTAGGTGGC	TCCTGCTTAAGTCCCTGGAG	This paper
<i>Il-4</i>	TGTCATCCTGCTCTTCTTTCTC	GCACCTTGGAAGCCCTAC	This paper
<i>Il-10</i>	GCATGGCCCAGAAATCAAGG	AGAAATCGATGACAGCGCCTC	This paper
<i>Ifn<math>\gamma</math></i>	GCTCTGAGACAATGAACGCTAC	TTCTAGGCTTTCAATGACTGTGCC	This paper
<i>Arg1</i>	GCAACCTGTGTCCTTTCTCC	TCTACGTCTCGCAAGCCAAT	This paper
<i>Nos2</i>	CTGCCTCATGCCATTGAGTT	TGAGCTGGTAGGTTCTGTTG	This paper
<i>Cxcr2</i>	ATCCACCTTGAATTCTCCCAT	GTCACAGAGAGTTGGGACCC	This paper
<i><math>\beta</math>-Actin</i>	GATCAAGATCATTGCTCCTCC TGA	CAGCTCAGTAACAGTCCGCC	This paper
Influenza Matrix Protein	CCCTGAAGTACCCCATGAAC	CTTTTCACGGTTGGCCTTAG	This paper

**Table S1. Primers used for quantitative PCR. Related to STAR Methods.**